Allosteric Interactions between DNA Strands and Monovalent Cations in DNA Quadruplex Assembly: Thermodynamic Evidence for Three Linked Association Pathways†

Charles C. Hardin,* Matthew J. Corregan, David V. Lieberman, and Bernard A. Brown II

Department of Biochemistry, North Carolina State University, Raleigh, North Carolina 27695

Received March 3, 1997; Revised Manuscript Received June 20, 1997⊗

ABSTRACT: The series of cooperative transitions that lead to $[d(TG_4)_4 \cdot (K^+)_m]$ quadruplex assembly upon rapid addition of KCl to $d(TG_4)$ strands were studied. Quadruplex samples were dialyzed against KCl then Li-EDTA and found to retain between three and five strongly bound potassiums with affinities $>10^6$ M^{-2}. Absorbance thermal denaturation (melt) and circular dichroism (CD) equilibrium binding data were obtained. The latter were analyzed using two classes of binding models to simulate the effects of the assumed intermolecular interactions on the binding curves (isotherms). The melt experiments yielded equilibrium dissociation constants (K_d) ranging from 10^{-11} to 10^{-12} M^3 at the melting temperatures. Extrapolating these values to 23 °C predicts K_d values in the 10^{-28} M^3 range if the heat capacity (C_p) is not strongly dependent upon temperature changes over this range. Assuming K_a is equal to $1/K_d$ (from melting analyses), very large association free energies stabilize the quadruplex at 23 °C in 100 mM KCl ($\Delta G_a = -43$ kcal mol^{-1}). Plots of the differential melt curve peak half-widths, a measure of cooperativity, versus $d(TG_4)$ concentration showed that quadruplex dissociation is much more cooperative at 400 mM KCl than at 100 mM KCl. Forty-eight hour quadruplex assembly time courses were monitored by CD at 264 nm. Equilibrium quadruplex accumulation generally required over 10 h, and net reaction extents were in the 10−85% range. Hill plots of the data show that initial steps in the multistep pathway are positively cooperative, presumably due to strong strand−cation and strand−strand binding interactions in duplex and triplex assembly reactions, then negatively cooperative in quadruplex formation. Models were developed to rationalize the experimental observations in terms of consecutive cooperative allosteric transitions from cation-deficient *relaxed* (R) strand-aggregates to cation-containing *tense* (T) structures, driven by the allosteric effector K^+. Quantitative mappings of positive and then negative cooperativity were obtained by fitting the results as a function of strand number incorporated during quadruplex assembly. Surprisingly, models for reactions involving incorporation of five and six strands fit the data better than models involving only four strands. The 5-step "induced fit" model fits the data as well as or better than 3- and 4-step models and better than all of the strand aggregation models that were devised and investigated. Net association free energies ($\sum_{i=1,n}\Delta G_i'$) ranged from −20 to −26 kcal mol^{-1}, approximately half the magnitude of the apparent stabilities measured by absorbance melts. Likely explanations for this discrepancy involve hysteresis and errors due to inadequate equilibration in the melt experiments. Hysteresis is thought to be produced by irreversibility due to different predominant mechanisms in absorbance (dissociation) and CD (association) experiments. The kinetic block to quadruplex assembly can be unambiguously attributed to quadruplex formation and not intermediate steps in the assembly mechanism. On the basis of these results we propose that, in addition to the more conventional assembly mechanisms involving duplex dimerization and stepwise strand addition, quadruplex formation can also proceed by triplex−triplex disproportionation. Interaction statistics arguments that support the energetic feasibility of the disproportionation pathway are presented. The allosteric quadruplex assembly model provides a mechanism which could be used by the cell to simultaneously modulate DNA structure and activity within telomeres, transcriptional promoters, recombination-prone chromatin, and other G-rich DNAs. As a result of this allosterism, cation and strand availability and strand-pairing capabilities could profoundly influence the functional capacity of a particular strand over a relatively narrow range of effector concentration changes. This is analogous to the control of enzymes in intermediary metabolism by the availability of allosteric effectors. By extension, allosteric effectors in quadruplex assembly can be classified as both facilitory and inhibitory. Future reports present examples of each. These relationships might contribute to understanding how cellular and nuclear homeostasis and genetic functions are linked.

Guanine-rich telomeric DNA sequences have been studied intensively since their intriguing cation-dependent self-assembling characteristics were first described [see reviews by Williamson (1994) and Vencenzel and Sen (1996)]. Guanine-cytosine-rich DNA sequences are found within at least three different functional domains in eukaryotic chromosomes: in highly repetitive sequences at the chromosomal termini (telomeric DNAs), in immunoglobulin switch region DNA sequences, and in "CpG islands" located

† Supported by National Institutes of Health Grants BRSG RR9223 and GM47431, a North Carolina Biotechnology Center ARIG Grant, and the North Carolina Agricultural Research Service.

* To whom all correspondence should be addressed.

⊗ Abstract published in *Advance ACS Abstracts,* November 1, 1997.

S0006-2960(97)00488-1 CCC: $14.00

in the coding and promoter regions of genes.

In vitro studies with G-rich telomeric DNA sequences have shown that they can form both intra- and intermolecular quadruplex structures (Sen & Gilbert, 1990; Hardin *et al.*, 1991; Miura *et al.*, 1995). The stabilities of these structures are uniquely sensitive to changes in the concentrations of important physiological cations such as K^+ and Ca^{2+}. On the basis of computational free energy perturbation calculations, monovalent cations bind with the following relative affinities within the cavity formed by the eight guanine "host" carbonyl oxygens (GO6) that surround each "guest" cation: $K^+ > Na^+ \approx Rb^+ > Cs^+ \geq Li^+$ (Ross & Hardin, 1994).

Potassium is the predominant monovalent cation in eukaryotic nuclei; Na^+ is present at less than half the K^+ concentration. While exact cation concentrations vary in different cell types, typical basal ranges are *ca.* 30 mM Na^+ and *ca.* 110 mM K^+ (Boynton *et al.*, 1982; Ling, 1984). The K^+ concentration increases from *ca.* 90 to 130 mM during the normal cell cycle. Patch−clamp studies of the mouse nuclear membrane suggest that nuclear K^+ concentrations are regulated by K^+ ATPase synports which are controlled *in vitro* by nucleotide cofactor concentrations (Mazzanti *et al.*, 1991; Bustamante, 1993). These results suggest that changes in potassium concentration could change chromatin structure by taking advantage of the unique sensitivity of quadruplex formation to Na^+ and K^+ concentrations. In theory, the cell could use physiological homeostasis and nuclear compartmentalization to drive intra- and interdomain binding interactions by ion-induced self-assembly reactions within chromosomes, especially within G-rich chromatin domains.

Telomere maintenance is associated with cell immortality (Hastie *et al.*, 1990; Kim *et al.*, 1994). This has led to the conclusion that telomerase inhibitors may be "effective anticancer drugs" (Borman, 1994). The mechanism proposed in the previous paragraph may be a significant link between the functional status of G-rich domains, such as those in telomeres, and the status of physiological growth factor-mediated processes, which could be dysfunctional in cancer cells.

Olivas and Maher (1995) found that cation and strand sequence can act synergistically to limit the extent of antisense triplex formation *in vitro*. Potassium was found to inhibit triplex formation by promoting a competing quadruplex formation reaction. Kandimalla and Agrawal (1995) found that foldback triplex-forming oligonucleotides can promote quadruplex formation. Oligonucleotide sequence, solution conditions, and temperature affected the predisposition of these processes, indicating their importance in determining whether such sequences are functionally effective in the quadruplex induction pathway.

An understanding of the protein components that modulate the functions of telomeres and other G-rich chromatin is beginning to emerge. Early findings with quadruplexes *in vitro* uncovered a protein chemistry that revolves in part around basic amino acids and guanidinium functionalities (Fang & Cech, 1993a,b). The *Oxytricha* telomeric DNA-binding protein β and a number of other polycationic proteins, including poly(L-lysine), promote quadruplex formation. The details of how the proteins facilitate association are not understood. Giraldo and Rhodes (1994) found that the ubiquitous yeast protein RAP1 binds to GT-rich telomeric DNAs and promotes intermolecular quadruplex assembly at nanomolar concentrations. To quote Giraldo and Rhodes (1994), this result "argues for the use [function] of DNA quadruplexes in telomere association" and as a "means for regulating the association and dissociation of telomeres". One goal of the present study is to develop a sufficiently realistic thermodynamic and mechanistic foundation for these complicated phenomena.

The oligonucleotide $d(T_2G_4T_2G_4T_2G_4T_2G_4)$ can form three different structures which, depending upon strand and cation concentrations and type of cation, are thought to contain either 1, 2, or 4 strands (Hardin *et al.*, 1991). Since strand folding interactions in the presence of cations play such an important part in the proposed mechanism of quadruplex formation in these aggregates, we set out to analyze the detailed thermodynamics and kinetics of quadruplex formation starting with the small asymmetric 4-stranded quadruplex $[d(TG_4)_4 \cdot (K^+)_{3-5}]$.[1] Despite the apparent simplicity of this system, the thermodynamic analysis is very complex and, as a result, not completely tractable.

This report provides a relatively thorough description of the quadruplex assembly reaction and characterizes thermodynamic linkages between the constituent subreactions involved in $[d(TG_4)_4 \cdot (K^+)_{3-5}]$ formation. Thermodynamic evidence is presented to support the existence of a complex "induced fit" assembly mechanism that proceeds by three linked pathways. Two are formally classified as *aggregration*: (1) stepwise strand addition and (2) duplex dimerization. The third route (3) involves *disproportionation* of a six-stranded species (formed by triplex dimerization) to produce the quadruplex and simultaneously cast off a duplex when the strand is passed from the donor triplex to the acceptor triplex.

MATERIALS AND METHODS

Sample Preparation. Oligonucleotides were synthesized using standard phosphoramidite methods, lyophilized to dryness from concentrated NH_4OH, resuspended in deionized distilled H_2O, and dialyzed extensively against 0.1 mM Li_2EDTA (pH 7). Samples were dried and resuspended in 0.5 mL of 0.1 mM Li_2EDTA (pH 7), then dialyzed extensively against 10 mM potassium phosphate (KP_i) (pH 7). Subsequent dialysis against 0.1 mM Li_2EDTA (pH 7) removed most of the residual KP_i. After quantitation by UV absorbance spectroscopy on a Shimadzu UV-160 spectrophotometer, samples were stored at −4 °C at *ca.* 15 mM $d(TG_4)$.

Equilibrium Dialysis of KCl Pre-Equilibrated Quadruplexes. Stock quadruplex samples (*ca.* 0.5−1 mL) were

[1] Abbreviations: AA, atomic absorption spectroscopy; AK model, Adair−Koshland "induced fit" model; α_a, net reaction extent of association reaction ($=1 - \alpha_d$); C-BK, Cornish-Bowden and Koshland; CD, circular dichroism; c_T, total $d(TG_4)$ concentration (including all strands incorporated into complexes); $\Delta(\partial\alpha_a/\partial T)_{\alpha=0.5}$, peak half-width of a differential plot of α_a vs temperature; EDTA, ethylenediaminetetraacetic acid; K_a, equilibrium association constant (calculated as $1/K_d$); K_d, experimentally determined equilibrium dissociation constant; K_i', intrinsic microscopic equilibrium dissociation (Adair) constant; KP_i, potassium phosphate; K_{T_m}, equilibrium association constant determined at the T_m; LISA, lattice-independent strand aggregation; MWC, Monod-Wyman-Changeux; ss, single-stranded; Tris-HCl, tris(hydroxymethyl)-aminomethane titrated with HCl; ts, transition-state; WC, Watson−Crick; ξ_a, extent of the association reaction (assumed to be equal to α_a); Y_a, fractional saturation of the "lattice" in the "induced fit" models; Y_Q, fraction of strands in quadruplex in the aggregation models.

dialyzed against four 1.5 L buffer changes over 22 h into 10 mM KCl containing 0.1 mM EDTA in a BRL microdialysis apparatus. Loosely bound K^+ was removed by extensive dialysis into Li_2EDTA at pH 7. Potassium concentrations in the [$d(TG_4)_4$)] samples were then determined by atomic absorption (AA) spectrometry on a Perkin-Elmer model 3100 AA spectrometer. The results indicated that externally bound condensed cations are replaced by Li^+ while internally bound K^+ remains bound.

Absorbance Thermal Denaturation of d(TG₄). Thermal denaturation traces for the quadruplex to single-strand transition were acquired on a Gilford Response II UV spectrophotometer equipped with a six-position thermocontrolled cuvette holder. Temperature ramps from 25 to 95 °C were used with a step interval of 0.1 °C and acquisition rate of 0.25 °C/min. All samples contained 100 mM Tris-HCl (pH 7) and either 100 or 400 mM KCl. The $d(TG_4)$ concentration was varied from 228 to 808 μM in 100 mM KCl and from 60 to 1260 μM in 400 mM KCl. DNA concentration changes were accommodated by using 10, 1, and 0.1 mm path length CD cells. Melting temperatures were determined at the maxima of differential melt plots which were generated using the Gilford Response II software.

The net reaction can be expressed as

$$n\ d(TG_4) + m\ K^+ \leftrightarrow [d(TG_4)_n{\cdot}(K^+)_m] \qquad (1)$$

We adopt the abbreviations ss (or S_1) for *single stranded* and Q (or S_4) for *quadruplex* species and assume reaction stoichiometries for K^+ and $d(TG_4)$ based on atomic absorbance measurements and the definition of a quadruplex. The net reaction is then

$$4\ ss + 3{-}5\ K^+ \leftrightarrow Q \qquad (2)$$

To obtain molar quadruplex concentrations, absorbance values were measured for freshly diluted quadruplexes in 100 mM Tris-HCl (pH 7) at 23 °C. The molar extinction coefficient at 260 nm for the undissociated species was determined from absorbances of fully associated samples of known initial ss concentrations. This was done by starting with a sample of quadruplex, measuring its absorbance, then melting it and measuring the absorbance of the single strands. Single-strand concentrations were determined using a single-strand extinction coefficient which was calculated by the nearest neighbor procedure (Cantor & Tinoco, 1965; Cantor *et al*., 1970). The extinction coefficient for quadruplex was calculated as $\epsilon_Q = 4(\epsilon_{ss})(A_Q/A_{ss})$, where A_Q is the absorbance of the quadruplex at 23 °C, and A_{ss} is the absorbance of the single strands at 80 °C: $\epsilon_{Q,23} = 5.22 \times 10^4\ M^{-1}\ cm^{-1}$. Fully intact quadruplex preparations are inferred under conditions in which the maximum concentration normalized CD ellipticity at 264 nm remains unchanged despite a 10-fold increase in oligonucleotide concentration [$\geq$1 mM $d(TG_4)$ under the conditions used here]. (The ellipticity remains proportional to the amount of strand added and $\Delta\epsilon_{264,Q}$ remains constant.)

Equilibrium constants for the transition shown in eq 1 were determined at the melting temperature (T_m) from absorbance melts. The van't Hoff relations (eqs 5 and 6) were used to determine the van't Hoff enthalpy for quadruplex association (ΔH_a) and predict extrapolated equilibrium constants at lower temperatures (Marky and Breslauer, 1987).

$$K_a = [Q]/[ss]^n = \alpha_a[n(c_T)^{n-1}(1-\alpha_a)^n]^{-1} \qquad (3)$$

$$K_{a,T_m} = [n(c_T/2)^{n-1}]^{-1} \qquad (4)$$

$$\frac{1}{T_m} = \frac{(n-1)}{\Delta H_a}\ln C_T + \frac{\Delta S_a - (n-1)R\ln 2 + R\ln n}{\Delta H_a} \qquad (5)$$

$$\ln[K_a(T)/K_a(T_m)] = (\Delta H_a/R)[(T^{-1}) - (T_m{}^{-1})] \qquad (6)$$

Note that quadruplexes are dissociated (relatively irreversibly) in our experiments, then we calculate K_a assuming it is equal to $1/K_d$.

The extrapolation in eq 6 assumes that the molar heat capacity C_p remains constant across the temperature range. Actually, ΔH_a and C_p might change significantly as one proceeds across the quadruplex melt curve (disassembly reaction coordinate). Because changes in C_p associated with protein temperature-dependent unfolding might be significant (Dill, 1990; Gomez & Friere, 1995) and similar effects might be expected for quadruplex dissociation, the extrapolated dissociation equilibrium constants and extrapolated ΔG_a and ΔS_a values shown in Table 2 must be considered approximate. They will be most reliable at the T_m and less so at other temperatures. Introduced errors are probably not large since ΔC_p and $(\partial\Delta H_a/\partial T)_p$ are typically small for unfolding−folding reactions of small globular proteins in the 20−60 °C range. Since the calorimetrically measured heat exchange due to phase transitions in this temperature range should be primarily due to solute structural transformations and not bulk H_2O phase changes, the trend for quadruplex association−dissociation is probably similar to that observed for proteins.

Quadruplex dissociation melt measurements were made as a function of KCl concentration ranging from 0 to 0.6 M at a constant DNA concentration of 600 μM. For comparison, the DNA concentration-dependent melt data described above were acquired at constant KCl concentrations of either 100 or 400 mM. Equations 3−6 were adapted to analyze the dissociation thermodynamics as a function of KCl concentration by assuming that three cations bound per quadruplex formed.

^{1}H NMR Spectroscopy. Proton NMR spectra of [$d(TG_4)_4$] samples were acquired as a function of temperature using the 1−1 hard-pulse solvent suppression technique on a 500 MHz GE Omega spectrometer. DNA quadruplex concentrations were *ca.* 0.2 mM, and samples contained 100 mM Tris-HCl (pH 7), 0.1 mM EDTA, and 1, 10, or 100 mM KCl in 0.6 mL of 10% D_2O/90% H_2O. Approximately 0.1 mM sodium TSP was included as chemical shift reference.

Circular Dichroism Equilibrium Association Isotherms. Transitions from dissociated $d(TG_4)$ strands to quadruplexes were monitored by CD at 264 nm on a Jasco J-600 spectropolarimeter. Temperature was controlled by recirculating water through cylindrical quartz CD cells from a Neslab water bath. Cell temperatures determined by thermocouple measurements did not differ from the bath temperature from 0 to 90 °C. A series of samples, with concentrations ranging from 5 to 300 μM $d(TG_4)$, were prepared in 100 mM Tris-HCl (pH 7). Under these conditions, at 23 °C, preformed [$d(TG_4)_4$] is stable despite dilution from milli- to micromolar concentrations, so samples were

heated at 80 °C for 30 min to denature the complexes to ss species ($S_1 = R_1 + T_1$, see Discussion). Samples were then cooled for 15 min before adding 100 mM KCl, then incubated at 37 °C for up to 48 h. At several intermediate times and at the end of the period, CD spectra were obtained for each sample at 37 °C and the ellipticity at 264 nm was determined.

We make three assumptions. (1) We assume that the observed change in molar ellipticity ($\Delta\theta_{obs} = \theta_{obs,final} - \theta_{obs,initial}$) can be attributed entirely to the change in quadruplex concentration. While this is correct as a first-order approximation, contributions to $[\theta]_{264}$ by intermediates engaged in quadruplex assembly would introduce error into quantitative analyses of the results. (2) We assume that $\Delta[\theta]_{264}$ is linearly dependent on the "tense" quadruplex concentration, $[T_4]$ ([Q]). (3) We assume that $\Delta[\theta]_{264}$ values measured after storing the samples at d(TG_4) concentrations between 2 and 5 mM then diluting to *ca.* 0.2 mM in 100 mM potassium phosphate (pH 7) correspond to a quadruplex mole fraction of unity. The *spectroscopically observed fraction bound* α_a is assumed to equal the fractional *extent of reaction* (ξ), which is assumed to equal 1 when all reactants and intermediates are converted to quadruplex. If any remaining nonquadruplex species in the solution contribute to $[\theta]_{264}$, the apparent $\Delta\theta_{obs}$ per mole of quadruplex will be larger than the assumed value. We determined the experimental CD at 264 nm per mole of strands incorporated into quadruplex to obtain our assumed $[\theta]_{264}$ value of 3.05 mdeg μM^{-1} cm^{-1}.

$$[\theta]_{264,Q} = 4\theta_{obs}/[S_1] \qquad (\alpha_a = 1) \tag{7}$$

This assumes that contributions due to CD spectra of intermediates engaged in the assembly process do not significantly perturb the ellipticity of the quadruplex. Under most circumstances used in this work, strands are not converted completely to quadruplex. The free energy minimum is typically achieved at $\alpha_a \approx 0.6-0.9$. Essentially complete conversion of S_1 to Q can be achieved by lowering the temperature and increasing the strand concentration.

Ellipticities were measured at 264 nm following a 48 h equilibration period at 37 °C in 100 mM Tris-HCl at pH 7. *Intrinsic (microscopic) equilibrium association constants* K_i' (also called Adair coefficients) were calculated by fitting the results to the following general equation:

$$\log\left(\frac{Y}{1-Y}\right) = \log\left\{\frac{\sum_{n=1}^{N} f\binom{N}{n}\left[\left(\prod_{i=1}^{n} K_i'\right)([C_T]^n)\right]}{1 + \sum_{n=1}^{N-1} f\binom{N}{n+1}\left[\left(\prod_{i=1}^{n} K_i'\right)([C_T]^n)\right]}\right\} \tag{8}$$

Y, the fractional saturation of the lattice, was set equal to Y_a (and assumed to equal α_a). Binomial expansion coefficients, $f\binom{N}{n}$, are (for $N = 4$) $f\binom{4}{1} = 1$, $f\binom{4}{2} = 3$, $f\binom{4}{3} = 3$, $f\binom{4}{4} = 1$; (for $N = 6$) $f\binom{6}{1} = 1$, $f\binom{6}{2,\ldots} = 5, 10, 10, 5, 1$; (for $n = 8$), $f\binom{8}{1,\ldots} = 1, 7, 21, 35, 35, 21, 7, 1$; and (for $N = 10$), $f\binom{10}{1,\ldots} = 1, 9, 36, 84, 126, 126, 84, 36, 9, 1$. The K_i' correspond to *n intrinsic association constants* as defined by Cornish-Bowden and Koshland (1975). To illustrate, letting A represent the lattice and X the ligand, for $N = 4$ the expression is

$$\log\left(\frac{Y}{1-Y}\right) = \log\left(\frac{K_1'C_T + 3K_1'K_2'C_T^2 + 3K_1'K_2'K_3'C_T^3 + K_1'K_2'K_3'K_4'C_T^4}{1 + 3K_1'C_T + 3K_1'K_2'C_T^2 + K_1'K_2'K_3'C_T^3}\right) \tag{9}$$

where $K_1' = [AX]/4[A][X]$, $K_2' = 2[AX_2]/3[AX][X]$, $K_3' = 3[AX_3]/2[AX_2][X]$, and $K_4' = 4[AX_4]/[AX_3][X]$.

Binding isotherms were fit to eq 9 using the SAS curve fitting program NLIN (SAS Institute, Cary, NC). Two different assumptions involving the amount of single strands (S_1) remaining at equilibrium were investigated: (*1*) $S_1 = c_T(1 - \alpha_a)$ and (*2*) $S_1 = c_T/4$. The former definition assumes for comparative purposes that significant amounts of duplex and triplex do not accumulate. The latter assumes that one-fourth of the strands always remain free, that significant amounts of triplex and duplex might accumulate and that $\alpha_a = 0.75$. Assumption 2 would be more appropriate at lower strand concentrations where there is insufficient chemical potential to drive extensive quadruplex formation, yet intermediates should accumulate ($\alpha_a < 0.5$; $S_1 \neq c_T - 4S_4$). Both assumptions produced results which indicate that the quadruplex formation step requires more energy than any other substep in the reaction.

Initial estimates were made by determining fits for stepwise microscopic association equilibrium constants (K_i'; Adair constants in eq 8) across a range of preliminary (coarse) solutions determined in an initial grid screen of the parameter space. Optimal sets of K_i' values were determined based on two criteria: (1) the Jacobian matrix could not be singular (all parameters used in the solution are sufficiently uncorrelated), and (2) fit curves gave a good visual approximation to the experimental results. While the latter criterion could be satisfied in some situations by using more parameters (*e.g.,* for $N \geq 6$ relative to $N = 5$), high correlation between K_n' values led to rejection of the fit.

Nonlattice aggregation binding models were also investigated. These models assume either stepwise strand addition, condensation of two duplexes, or a mixture of these two assembly pathways. Detailed descriptions, including statistical factors which take into account different strand binding and removal mechanisms, are given in the Appendix.

Nomenclature. The nomenclature used to indicate repetitive sequence DNAs within and apart from two- and higher stranded complexes can be ambiguous. Brackets generally indicate complexes in IUPAC nomenclature. Consider $[d(TG_4)]_4$. Placing the subscripted 4 outside the brackets (which is meant to indicate that four strands are in the complex) is clearly incorrect usage. Placing the subscripted 4 within the brackets can imply that TG_4 is repeated four times, which is not correct. To be unambiguous, we advocate writing out the entire sequence of a strand, contracting repeated nucleotides using subscripts (*e.g.*, GGGT → G_3T), and reserving the subscript outside the parentheses and within the brackets to indicate the number of strands per complex. For example, $[d(TG_4TG_4)_3]$ refers unambiguously to a triple helix composed of three d(TG_4-TG_4) strands, containing two TG_4 repeats each. Our complex $[d(TG_4)_4]$ contains 4 d(TG_4) strands.

Table 1: Melting Temperatures of $[d(TG_4)_4 \cdot (K^+)_{3-5}]$ Determined from Temperature-Dependent Absorbance Changes at 260 nm Measured as a Function of [DNA] and $[K^+]$

100 mM KCl[a]		400 mM KCl[a]	
$[d(TG_4)]$ (μM)	T_m (°C)[b]	$[d(TG_4)]$ (μM)	T_m (°C)[b]
228	65.6	61.6	73.0
348	67.1	136.4	75.6
400	68.0	139.2	75.9
504	68.5	175.2	77.9
540	68.9	284.4	78.8
604	68.5	386.8	80.3
632	69.0	536	81.4
716	69.3	760	83.5
768	69.2	1260	86.4
808	70.3		

[a] Determined in 100 mM Tris-HCl, pH 7. [b] Standard errors were <0.5 °C in duplicate determinations.

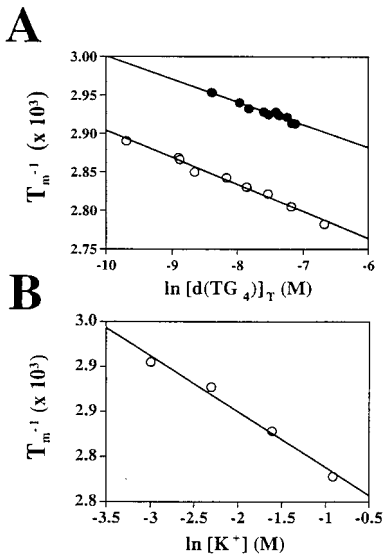

FIGURE 1: Van't Hoff analyses of absorbance thermal denaturation results for the quadruplex $[d(TG_4)_4]$. (A) Absorbance melts were measured as a function of $[d(TG_4)_4]$ concentration at constant KCl concentration. Reciprocal melting temperatures (T_m^{-1}) from $[d(TG_4)_4]$ thermal denaturation profiles are plotted as a function of log C_T (Marky & Breslauer, 1987). Samples contained 100 mM Tris-HCl (pH 7) and either 100 mM (●) or 400 mM (○) KCl; $d(TG_4)$ concentrations ranged from 57 to 202 μM in the 100 mM KCl samples and from 15 to 315 μM in 400 mM KCl. Linear regression R^2 values and slopes are listed in Table 2. (B) Van't Hoff plot of T_m^{-1} values plotted as a function of the KCl concentration. Samples contained 150 μM $d(TG_4)$ and 100 mM Tris-HCl (pH 7). R^2 and the slope are listed in Table 4B.

RESULTS

Quadruplex Dissociation Thermodynamics: d(TG$_4$) Concentration Dependence. Absorbance thermal denaturation (melt) data obtained at 260 nm were used to determine "equilibrium" quadruplex association constants assuming $K_a = 1/K_d$. The temperature was raised from 25 to 95 °C at 0.25 °C min^{-1}. All thermal denaturation curves were approximately monophasic (results not shown). T_m values, corresponding to peak maxima of first derivative melt plots, were determined at 100 and 400 mM KCl to determine the sensitivity of the results to K^+ concentration. Results are listed in Table 1.

Plots of T_m^{-1} versus ln c_T were constructed to determine dissociation enthalpies (Figure 1A) by following standard protocols (Marky and Breslauer, 1987). *Equilibrium association constants* (K_a) were calculated from dissocation results at the respective T_m values (where the *fraction of dissociated quadruplexes* α_d is equal to 0.5) according to eq 5 of Marky and Breslauer (1987). Oligonucleotide concentrations in Table 1A and a quadruplex strand stoichiometry of 4 were used. Similar analyses of quadruplex melt data obtained with other sequences have appeared (Jin *et al.*, 1990; Guo *et al.*, 1993; see below).

Table 2: Dissociation Constants for $[d(TG_4)_4 \cdot (K^+)_{3-5}]$ Determined from Absorbance Melt Results and Inferred Association Constants in 100 and 400 mM KCl[a]

$[d(TG_4)]_T$ (μM)	$[KCl]_T$ (mM)	T (°C)	$d(T_m^{-1})/d(\ln c_T)$[b]	K_d (M^3)[c]	K_a (M^{-3})[d]
808	100	70.3	-2.970×10^{-5}	4.12×10^{-12}	2.43×10^{11}
387	400	80.3	-3.504×10^{-5}	4.52×10^{-13}	2.21×10^{12}
808	100	37		7.75×10^{-26}	1.29×10^{25}
387	400	37		1.87×10^{-29}	5.35×10^{28}
808	100	23		1.57×10^{-32}	6.37×10^{31}
387	400	23		4.17×10^{-37}	2.40×10^{36}

[a] Determined in 100 mM Tris-HCl (pH 7) at the stated reactant concentrations; initial quadruplex concentrations were assumed to be equal to the total $d(TG_4)$ concentration divided by 4. [b] Slopes obtained by linear regression of the respective van't Hoff plots; R^2 values were 0.987 for the 100 mM KCl data and 0.954 for the 400 mM KCl results. c_T refers to the total strand concentration. [c] Equilibrium constants calculated by extrapolation from values obtained at T_m according to eq 6 assuming that the van't Hoff slope remains constant over the temperature range. [d] Calculated as $K_a = 1/K_d$ assuming that association and dissociation are reversible.

Experimentally determined K_a values (taken to be $1/K_d$ in eqs 3 and 4), van't Hoff slopes (Figure 1A), and calculated *equilibrium association constants determined at the T_m* (K_{T_m}) are listed in Table 2. The expression for the Q formation equilibrium, which includes strands and Q if no intermediates accumulate, is: 4ss → Q; $K_a = [Q]/[ss]^4$; the dimensions are M^{-3}. Units of K_d are cubic molarity.

The van't Hoff treatment requires that the heat capacity C_p of the system remain unchanged within the extrapolated temperature range. Under this assumption, dissociation equilibrium constants were predicted by extrapolating values determined at 100 and 400 mM KCl at the respective T_ms to 37 and 23 °C (Table 2). Remarkably, at 100 mM KCl and 0.81 mM $d(TG_4)$, K_a values ($1/K_d$) are predicted to increase from 2.4×10^{11} to 6.4×10^{31} M^{-3} when the temperature is reduced from 70 to 23 °C (Table 2). These complexes are exceptionally stable.

Association free energies (ΔG_a) calculated from the extrapolated equilibrium constants are listed in Table 3. *Entropic contributions to these association free energies* ($-T\Delta S_a$) were calculated using ΔG_a and ΔH_a in the Gibbs equation (Table 3). The total free energy and thermodynamic contributions due to ΔH_a and $-T\Delta S_a$ obtained by extrapolation to 37 and 23 °C are also listed in Table 3.

In general, enthalpic contributions to the overall free energy stabilize the quadruplex while entropic contributions are destabilizing (Table 3). For example, in 100 mM KCl at 70 °C, ΔG_a for $[d(TG_4)_4]$ association (at 808 μM strand concentration) is equal to −18 kcal mol^{-1}, the result of an inferred association enthalpy (ΔH_a°) of −201 kcal mol^{-1} and free energy contribution due to entropy ($-T\Delta S_a^\circ$) of 183 kcal mol^{-1}. Excess stabilizing enthalpies relative to destabilizing entropy-derived free energies produce the overall stabilization. This is reasonable considering the large amount of order in an intact quadruplex and the large amount

Table 3: Van't Hoff Quadruplex Association Thermodynamics for $[d(TG_4)_4 \cdot (K^+)_{3-5}]$ Determined from Absorbance Melt Results at 100 and 400 mM KCl[a]

$[d(TG_4)]_T$ (μM)	$[KCl]_T$ (mM)	T (°C)	ΔG_a (kcal mol^{-1})	ΔH_a (kcal mol^{-1})	$-T\Delta S_a$ (kcal mol^{-1})
808	100	70.3 (T_m)	−17.9	−200.7	182.8
387	400	80.3 (T_m)	−17.5	−170.1	152.6
808	100	37.0	−35.6	−200.7	165.1
387	400	37.0	−40.8	−170.1	129.3
808	100	23.0	−43.1	−200.7	157.6
387	400	23.0	−49.3	−170.1	120.8

[a] Thermodynamics were determined with respect to $d(TG_4)$ concentration liberated assuming four strands dissociate per quadruplex, that the reaction is reversible and that $\Delta C_p = 0$. The ΔS_d values were calculated using (1) the measured ΔH_a (at T_m, and assuming $d\Delta H_a/dT = 0$), (2) K_{a,T_m} and the van't Hoff relations to obtain K_a (assumed to be K_d^{-1}) at other temperatures, and (3) calculated ΔG_a ($-RT \ln K_d^{-1}$).

of freedom gained by the strands upon dissociation. The difference between these contributions increases upon extrapolation to lower temperatures, resulting in stabilizing free energies between −43 and −50 kcal mol^{-1} at 23 °C (Table 3), depending upon the KCl and strand concentrations. The quadruplex was more stable at 400 mM KCl than at 100 mM KCl even though the DNA concentration was lower.

Complications might be expected as a result of using Tris in the melt experiments. The change in pK_a of Tris might be as much as 2 units upon increasing the temperature from 25 to 95 °C ($pK_a = 8.3$, $dpK_a/dT = 0.031$ °C^{-1}). The pH region from about 5.5 to 8.5 in a plot of *observed assembly rate constant* versus *pH* (for two resolved relaxation subprocesses) is relatively flat. Since the assembly rate constants and assembly equilibrium constants show parallel behaviors, we surmised that the equilibrium constants for quadruplex assembly at pH 7 should not be particularly sensitive to expected pH changes upon melting due to the temperature dependence of Tris. Denaturation and assembly reactions do not occur with equal ease due to a large kinetic barrier to assembly (k_a is $\gg k_d$; manuscript in preparation). Therefore, we cannot place much quantitative confidence in the thermodynamic information obtained in the melt experiments, where the temperature coefficient of Tris would be problematic.

We include the melt data because (1) they are semiquantitatively accurate, (2) they agree with those of Guo et al. (1993) (which were also obtained under "irreversible" melting conditions), (3) they address the linked effects of strand and KCl concentrations, and (4) by comparison with the assembly results, provide quantitative evidence for the magnitude of the hysteresis effect in determined K_a and K_d values. Our CD quadruplex assembly data were all obtained at 37 °C and are thus unaffected by the temperature dependence of Tris.

Jin et al. (1990) provide an example of reversible quadruplex assembly data (from melts in 1 M KCl) and thermodynamic analyses for the $[d(G_2T_5G_2)_4] \leftrightarrow 4\ d(G_2T_5G_2)$ equilibrium. Their higher salt concentration is more conducive to association and less so to dissociation than that used by Gao et al. (1993) and in the present study (100−400 mM).

Our treatment can only be considered approximate due to the relatively rapid time frame used to acquire the denaturation data (0.25 °C min^{-1}). The T_m values and widths of the differential melt curves are strongly dependent upon sample concentration. In addition, complexes do not readily reform when samples are cooled to ambient temperatures.

These observations provide evidence for cooperativity between strands in the quadruplex dissociation process and indicate that the equilibrium is not readily reversible under these circumstances.

Key issues that must be addressed to calculate (the most) "correct" K_a values revolve around corrections due to possible accumulated reaction intermediates and differences in predominant mechanism in the assembly and denaturation reactions. Detailed dual-wavelength kinetic studies demonstrate that accumulation and dissipation of intermediates can be documented, but only semiquantitatively (manuscript in preparation). The work suggests that the amounts of accumulated intermediates are not large enough to seriously alter the two-state behavior of the denaturation results, especially in the positively cooperative denaturation direction.

Three different types of quadruplex assembly reactions are thought to occur via different final steps: single strand-triplex aggregation, duplex dimerization, and disproportionation of a pair of triplexes to form a quadruplex and duplex. The corresponding reverse dissociation reactions involve (1) disassembly of the quadruplex to produce a triplex and strand or two duplexes (see Figure 10), or (2) reverse-disproportionation (comproportionation). Hypothetical comproportionation involves end-to-end [quadruplex·duplex] formation then strand passage from quadruplex to duplex to produce a pair of triplexes (Figure 11).

Kinetic studies (manuscript in preparation) provide evidence which suggests that $[d(TG_4)_4]$ assembly is mostly due to duplex dimerization and to a lesser extent to stepwise strand addition, but that a small percentage ($\leq$15%) of quadruplex is produced by disproportionation of two triplexes. In contrast, $[d(TG_4)_4]$ dissociation is probably almost exclusively the result of successive strand losses or dissociation to form two duplexes. Reverse-disproportionation of duplex and quadruplex species to form two triplexes is probably rare because duplex-quadruplex encounters are unlikely compared to complexes with the same number of strands.

Xu *et al.* (1993), Williamson (1994), and Wyatt *et al.* (1996) found that quadruplex dissociation occurs slowly, suggesting the presence of a high activation energy barrier. On the basis of CD association kinetics results, quadruplex assembly does not achieve thermal equilibrium at each temperature during absorbance melt data acquisition, so dissociation is not strictly reversible relative to the assembly process. If the aggregation pathways predominate in both directions and occur in similar proportions, the reaction is mechanistically reversible in a microscopic sense. If one pathway is more predominant or excluded in one direction relative to the other, the equilibrium is not strictly reversible. As a result, without sufficient knowledge regarding the mechanistic features and reaction predispositions in both directions, one cannot confidently infer accurate information regarding quadruplex assembly based on quadruplex dissociation thermodynamics determined from absorbance melt results [*e.g.*, Guo *et al.* (1993), Wyatt *et al.* (1996), and Hud *et al.* (1996)].

Dissociation Thermodynamics Determined as a Function of KCl Concentration. Absorbance melt data were acquired by varying the KCl concentration (0−0.6 M) at 150 μM $d(TG_4)$ in 100 mM Tris-HCl (pH 7) (Figure 1B; Table 4).

Table 4: Thermodynamics for $[d(TG_4)_4 \cdot (K^+)_{3-5}]$ Association Inferred from Absorbance Melt Results as a Function of KCl Concentration

A. Effect of KCl Concentration on the T_m for $[d(TG_4)_4 \cdot (K^+)_3]$ Dissociation

$[K^+]$ (mM)[a]	T_m (°C)
0	35.6
50	65.3
100	68.6
200	74.3
400	80.5

B. Van't Hoff Dissociation Constants and Inferred Association Constants

[KCl] (mM)	T (°C)	$d(T_m^{-1})/d(\ln c_T)$[b]	K_d (M^2)[c]	K_a (M^{-2})[d]
100	68.6 (T_m)	-6.203×10^{-5}	7.50×10^{-3}	133.3
100	37		4.98×10^{-7}	2.01×10^6
100	23		3.64×10^{-9}	2.75×10^8

C. Van't Hoff Association Thermodynamics Extrapolated to 37 and 23 °C[e]

[KCl] (mM)	T (°C)	ΔG_a (kcal mol^{-1})	ΔH_a (kcal mol^{-1})	$-T\Delta S_a$ (kcal mol^{-1})
100	68.6	−3.32	−96.10	60.74
100	37.0	−8.94	−96.10	55.13
100	23.0	−11.43	−96.10	52.64

[a] Determined at 100 mM Tris (pH 7) and 150 μM $d(TG_4)$. [b] Slope obtained by linear regression of the van't Hoff plot as a function of KCl concentrations; R^2 was 0.984. Standard errors were <0.5 °C in duplicate determinations. [c] Equilibrium constants calculated by extrapolation from values obtained at T_m according to eq 5, assuming that the van't Hoff slope remains constant over the extrapolated temperature range ($\Delta C_p = 0$). Units are in terms of total K^+ bound per Q assuming a molecularity of 3 (see text). [d] Calculated as $K_a = 1/K_d$ assuming that dissociation is reversible. [e] Thermodynamics determined as described in Table 3.

K_a values for K^+ binding to the quadruplex were obtained from T_ms, determined as a function of KCl concentrations, by assuming that three cations bind per quadruplex and $K_d = 1/K_a$.

When m K^+ ions bind (and no intermediates accumulate), the net reaction is $4\ S_1 + m\ K^+ \rightarrow Q$; $K_a = [Q]/[S_1]^4[K^+]^m$; the dimensions of K_a are $(molarity)^{-(3+m)}$ (for $m = 3$, the dimensions are M^{-6}). Since the quadruplex dissociation reactions all contained the same amounts of $d(TG_4)$ and the amount of KCl was varied in these experiments, the K_d values in Table 4 only apply for K^+ binding at 150 μM $[d(TG_4)]_T$. The appropriate reaction is $4\ S_1 + 3\ K^+ \leftrightarrow [(S_1)_4 \cdot (K^+)_3]$, where $4\ S_1$ and $(S_1)_4$ refer to the spectator DNA strands in ss and Q. The dimensions of K_a are $(molarity)^{-2}$ (in K^+ only).

Melting temperatures (Table 4A) and the van't Hoff slope (Figure 1B; Table 4B) were determined as described for [DNA] dependence results. Equilibrium constants were extrapolated to 37 and 23 °C by assuming that C_p is temperature independent (Table 4B). Thermodynamic contributions to dissociation at the T_m and values obtained by extrapolation to 37 and 23 °C are listed in Table 4C.

As expected, the T_m increases with increased KCl concentration (Table 4A). This analysis produces an inferred K_a ($1/K_d$) for K^+ binding, upon extrapolation to 37 °C, of 2×10^6 M^{-2} (Table 4B). Cations are bound within the quadruplex with reasonably high affinity. This corresponds to a binding free energy (ΔG_a) of −8.9 kcal/mol of cation bound at 37 °C (Table 4C). As discussed in the previous section, this assumes that the dissociation reaction is reversible, so the results are only approximate. Contributions to the net free energies due to enthalpies and entropies conformed to the same pattern as found for the DNA-dependent melts. Enthalpic contributions stabilize the quadruplex more than entropic contributions destabilize it. As with strands, cations will be much more ordered within the quadruplex than in solution, so entropic factors should also strongly oppose quadruplex formation.

Table 5: Stoichiometry of Tightly Bound K^+ in $[d(TG_4)_4 \cdot (K^+)_m]$

determination	m $K^+/[d(TG_4)_4 \cdot (K^+)_m]$[a]	$m_{avg} \pm \sigma$
1 − Q	3.71	4.58 (±0.62)
	4.93	
	5.09	
2 − Q	3.77	3.55 (±0.22)
	3.33	
m average		4.07 (±0.84)
ss control[b]		0.08 (±0.11)

[a] Stoichiometries (m ± standard deviation) calculated from $[K^+]$ determined by atomic absorption spectrometry, and [DNA] determined by absorbance spectrometry at 260 nm. Samples were prepared by dialyzing quadruplexes into 10 mM potassium phosphate (pH 7) then 0.1 mM Li_2EDTA (pH 7) at 23 °C. [b] Average and standard deviation for three single-stranded samples produced as described in the Materials and Methods.

Comparing the inferred K_a values obtained with respect to KCl concentration (Table 4B) with those obtained with respect to $d(TG_4)$ concentration (Table 2) indicates that strands are much more responsible for the overall stability of the quadruplex than bound K^+. Strand binding free energies are approximately 4-fold larger than KCl-dependent ΔG_a values (−49.3 kcal mol^{-1} versus −11.4 kcal mol^{-1} at 23 °C).

The assumed K^+ stoichiometry of 3 per quadruplex is smaller than the average value determined by exhaustive dialysis against 0.1 mM Li_2EDTA followed by AA spectroscopy, 4.1 ± 0.4 (see below; Table 5). Since extensive dialysis may not "scrub the quadruplex clean" of externally bound K^+, it is reasonable to assume that the lowest value obtained by atomic absorption (3.3) is closest to the true number of internally bound K^+ ions. Only three cations bind to $[d(TG_4)_4]$ if the sites located between the four G-quartets constitute the only high affinity binding sites.

Four bound cations per quadruplex might also be possible. A "T-quartet" contains an [imino hydrogen·carbonyl oxygen] hydrogen-bonding pattern that is somewhat analogous to the site on the face of a G-quartet (Sarma *et al.*, 1992; Cheong & Moore, 1992). As a result, an extra lone pair electron on the T carbonyl oxygen might be available for ligation with a fourth internally bound cation in the space between the 5′-terminal G- and T-quartets. Depending on the sequence and type of structure, two T·T base pairs might also encourage cation binding (Ross & Hardin, 1994). Given the uncertainties, we list the range of bound K^+ as 3−5: $[d(TG_4)_4 \cdot (K^+)_{3-5}]$.

Cooperativity in Quadruplex Dissociation. "Differential melt" plots were obtained by calculating linear slopes using successive temperature versus α_a data pairs from the absorbance melt data sets. The half-width of the differential melt curve, $\Delta(\partial\alpha_a/\partial T)_{\alpha=0.5}$, is the temperature difference determined at half-height. This half-width parameter is a measure of the average behavior of the reaction component populations with respect to temperature changes and is related to the degree of cooperativity in the dissociation process (Marky

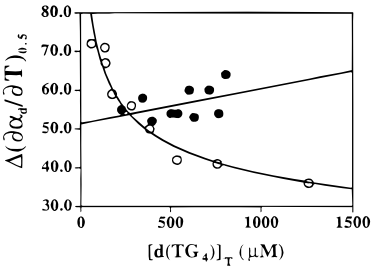

FIGURE 2: Evidence for cooperativity: DNA quadruplex differential thermal denaturation profiles. Reactions were monitored as a function of $[d(TG_4)_4]$ concentration in 100 mM Tris-HCl (pH 7) containing either 100 mM (●) or 400 mM (○) KCl. Differential melt profiles were calculated analytically from thermal denaturation data at the indicated $d(TG_4)$ concentrations. Half-widths of these differential melt profiles correspond to the temperature ranges that are spanned by the differential melt peaks at half-height, $\Delta(\partial\alpha_d/\partial T)_{0.5}$. More cooperative quadruplex denaturation occurs over a narrower temperature range, which produces a smaller $\Delta(\partial\alpha_d/\partial T)_{0.5}$ value. The 100 mM and 400 mM KCl data were fit to linear and exponential decay equations, respectively, solely to indicate the general trends.

& Breslauer, 1987). Strand or cation concentration changes shift populations across the range of temperatures corresponding to the maximum in the differential melt curve, the equilibrium "switchover temperature", where $\alpha_d = 0.5 = \alpha_a$ (Marky & Breslauer, 1987; Wyman & Gill, 1990). Association predominates at lower temperatures; dissociation predominates at higher temperatures; reactant and product components are distributed equally at the switchover temperature, which is by definition the T_m.

Since microscopic steps in the overall reaction might have very different energetic predispositions to occuring, the differential melt profiles need not be symmetric about the T_m. To a first approximation, they were symmetric in the case of $[d(TG_4)_4]$ dissociation. A narrower differential melt curve produces a smaller half-width. In this case, fluxes through intermediate states in the dissociation reaction are more dependent upon temperature changes. Decreasing $\Delta(\partial\alpha_a/\partial T)_{\alpha=0.5}$ values for quadruplex dissociation indicate that the process becomes more cooperative; increasing values correspond to less cooperativity.

Peak half-widths, $\Delta(\partial\alpha_a/\partial T)_{\alpha=0.5}$, are plotted as a function of DNA concentration for $[d(TG_4)_4]$ dissociation reactions in Figure 2. Trends obtained at 100 and 400 mM KCl are shown. The degree of cooperativity varies with DNA concentration. The 400 mM KCl results were fit to an exponential decay function to highlight the trend toward a narrower temperature range, consistent with more cooperativity in dissociation at elevated DNA concentrations in 400 mM KCl.

The 100 mM KCl samples melted with approximately equal degrees of cooperativity in experiments done across the 50−200 μM $d(TG_4)$ concentration range (Figure 2). In fact, a slight increase in $\Delta(\partial\alpha_a/\partial T)_{\alpha=0.5}$ is evident at higher DNA concentrations, indicating a slight loss in cooperativity. The 100 and 400 mM KCl curves overlap at *ca.* 19 μM $[d(TG_4)_4]$. This confirms that the strand and cation components are allosterically linked.

Equilibrium Dialysis: Internally Bound Potassiums. Does a population of K^+ remain tightly bound within the quadruplex in preference to exchange with solvent cations despite exhaustive dialysis against Li^+-containing solutions? The structure of the complex suggests that three potassiums bind internally with very high affinity [see Ross and Hardin (1994)]. To investigate this question, we dialyzed the quadruplex exhaustively against 0.1 mM Li_2EDTA (pH 7) in an effort to measure only the most tightly bound potassiums.

Ammonium (NH_4^+) has essentially the same van der Waals radius as K^+ and may remain bound within the quadruplex following removal of synthetic protecting groups from newly synthesized oligonucleotides with concentrated aqueous NH_4OH. Work with quadruplexes formed by poly(inosine) strands showed that NH_4^+ remains bound within the structure and stabilizes the complex about as well as K^+ (Howard & Miles, 1982). To minimize this possibility, bound NH_4^+ was replaced by dialyzing the samples extensively against 100 mM KCl prior to the EDTA dialysis.

If potassiums bind within $[d(TG_4)_4 \cdot (K^+)_{3-5}]$ with K_a values above *ca.* 10^6 M^{-2}, the binding sites should be essentially fully occupied in ≥100 mM KCl. Potassium-dependent melt results (Table 4B) indicate that this is likely to be the case. Samples were dialyzed against 100 mM KCl in 100 mM Tris-HCl (pH 7) to pre-equilibrate the quadruplex with K^+, then against 10 mM LiCl (pH 7) containing 0.1 mM Li_2-EDTA. Bound potassium content was determined by atomic absorption spectrometry. DNA strand content was determined based on absorbance measurements at 260 nm (see Methods). On the basis of CD results obtained under the same conditions, we inferred that essentially all of the strands were incorporated into quadruplex and that the ratio of K^+ to $0.25[d(TG_4)]_T$ equals the ratio of internally bound potassium atoms to quadruplex. Results shown in Table 5 indicate that $m = 3-5$.

Equilibrium may not be achieved in the "equilibrium dialysis" experiments. "Exhaustive dialysis" is probably a more appropriate term for our procedure. "Irreversibly melted" quadruplex samples (single strands) were dialyzed against LiCl until the external K^+ concentration was very low. All ss samples retained < 0.1 K^+ per strand (results not shown), while the quadruplexes retained the numbers listed in Table 5. The results depend upon two factors, the kinetic barrier to dissociation of internally bound K^+ and the ability of Li^+ to competitively displace internally bound K^+.

^{1}H NMR Spectroscopy. The ^{1}H NMR spectrum of $[d(TG_4)_4]$ in 10 mM sodium phosphate (pH 7), 1 mM EDTA at 20 °C has four well-resolved peaks in the imino proton region (10.2−11.2 ppm; see Supporting Information). These results indicate that $[d(TG_4)_4]$ is a stable quadruplex under these circumstances. Similar results have been obtained with the quadruplex formed by $d(T_2G_4T)$ (Wang & Patel, 1992; Xu *et al.*, 1993).

CD Quadruplex Assembly Reaction Time Course. To learn about the contributions of intermediate processes, quadruplex formation was studied in detail using equilibrium and kinetic CD measurements. These measurements are superior to absorbance measurements because they are more sensitive and allow one to better resolve signals due to different processes [*e.g.*, Hardin *et al.* (1992)]. CD association data were acquired as a function of $d(TG)_4$ concentration in 100 mM Tris-HCl (pH 7) containing 100 mM KCl. Potassium-induced association of $d(TG_4)$ was monitored in 100 mM Tris-HCl (pH 7) buffer containing 100 mM KCl at 37 °C and data were acquired in 0.1, 1, and 10 mm CD cells. Calculated *fractions of strands assembled into quadruplex*

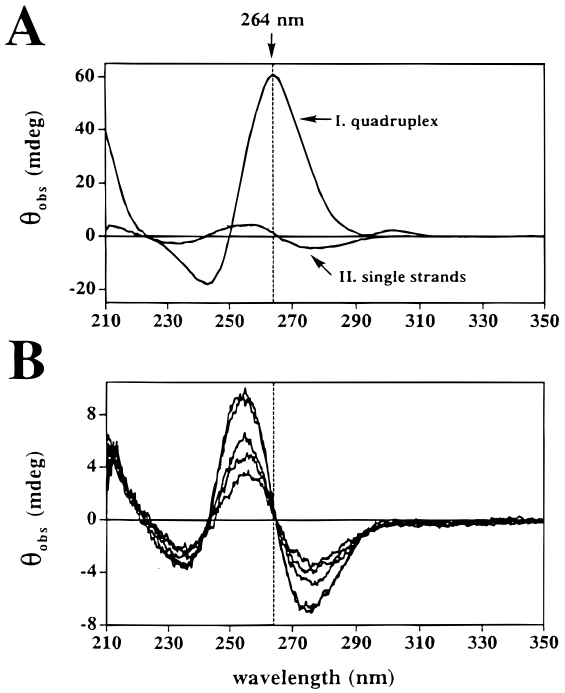

FIGURE 3: (A) Circular dichroism spectrum of $[d(TG_4)_4 \cdot (K^+)_{3-5}]$ in 100 mM Tris-HCl (pH 7), 0.1 mM EDTA at 23 °C (I) before and (II) after thermal denaturation at 80 °C for 30 min then returning the sample to 23 °C. Curve A corresponds to >95% metastable, intact DNA quadruplex; curve B corresponds to >95% single-stranded $d(TG_4)$. The dotted line at 264 nm shows the magnitude of the CD change that was monitored to study quadruplex assembly. Note that the $d(TG_4)$ single-strand spectrum has nearly zero ellipticity at 264 nm. The $d(TG_4)$ concentration is 150 μM. (B) CD spectra of single-stranded $d(TG_4)$ (trace II in panel A) obtained after melting the metastable quadruplex and cooling the sample to 20 °C, but not reassembling the complex. The upper spectrum at 255 nm was obtained at 20 °C before melting. Spectra were obtained during the second melt at 60, 50, and 40 °C (from least to third least intense spectra at 264 nm) and at 20 °C after the first and second melt, respectively (the two most intense spectra at 264 nm). Comparison of the latter two spectra indicates that the structural transition associated with the second melt is almost completely reversible.

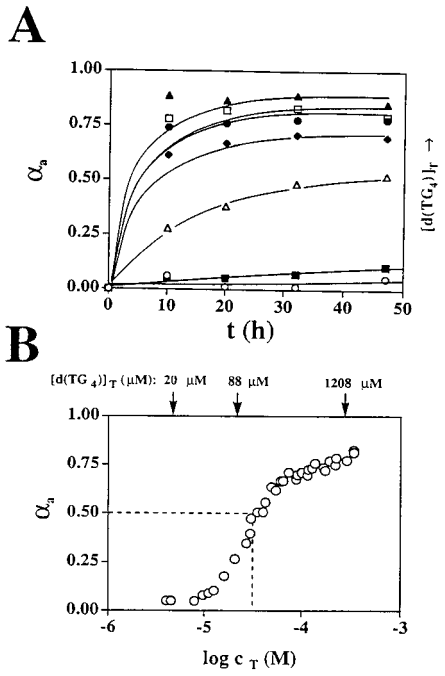

FIGURE 4: Circular dichroism equilibrium quadruplex assembly isotherms at 37 °C. (A) Association curves are shown for the following $d(TG_4)$ concentrations: (○) 4.4 μM, (■) 12.2 μM, (△) 39.4 μM, (◆) 85.5 μM, (●) 0.133 mM, (□) 0.187 mM and (▲) 0.326 mM. Samples were prepared by incubating DNA in 100 mM Tris-HCl (pH 7) at 80 °C for 30 min, cooling to 37 °C for 10 min, adding 100 mM KCl and incubation at 37 °C for up to 48 h. The fraction of $d(TG_4)$ that assembles into quadruplex, α_a, is plotted as a function of incubation time. (B) Assembled strand fractions α_a obtained after 48 h are plotted as a function of the total strand concentrations in reactions which include those shown in panel A.

α_a ranged from 0 to *ca.* 0.9 (assuming they are equal to *assembly reaction extents* ξ).

Results shown in Figures 3 and 4 demonstrate that thermal denaturation of the quadruplex is reversed by adding KCl to the sample. The CD of the DNA at 264 nm, $[\theta]_{264}$, before and after thermal denaturation is shown in Figure 3A. Two features of the spectra changed during quadruplex dissociation; the intensity at 264 nm decreased substantially and the maximum positive ellipticity in this range shifted to 255 nm. The simplest interpretation is that the loss of 264 nm ellipticity monitors quadruplex loss and that the intensity of the 255 nm band might be used to moniter single strand formation.

Figure 3B shows the temperature dependence of the spectrum of single-stranded $d(TG_4)$. The ellipticity at 255 nm decreases to less than half the value obtained at 20 °C when the temperature is raised to 60 °C. This behavior is consistent with a large loss of stacking interactions at 60 °C which are much more intact at 20 °C (Vesnaver & Breslauer, 1991). These stacking interactions reform rapidly and almost completely when the temperature is returned to 20 °C. Unlike quadruplex dissociation, loss of stacking is reversible under these conditions.

The situation would be more complicated if single strand buildup changed the value of $[\theta]_{264}$ substantially (manuscript in preparation). Fortunately, 264 nm represents a (nearly) zero ellipticity crossover point in the spectrum of the apparent single-stranded species. Thus, it remains essentially isoelliptic, independent of the status of the single-stranded population, and gives a reasonably accurate assessment of the change in quadruplex population upon association or dissociation. In contrast, changes in quadruplex concentration strongly affect $[\theta]_{255}$. As a result, $\theta_{obs,\ 255}$ cannot be used directly to monitor ss concentrations in samples that contain both ss and Q.

Figure 4A shows selected quadruplex association time courses monitored by following the CD of the DNA at 264 nm, $[\theta]_{264}$, after adding 100 mM KCl. Strand concentrations ranged from 5 to 350 μM; Tris-HCl buffer was used to obtain equilibrium data under the conditions used in the assembly kinetics studies (manuscript in preparation). (The samples also contained 100 mM Tris-HCl (pH 7) and 0.1 mM Li_2-EDTA to buffer against pH changes and sequester divalent cations, respectively.)

Measured α_a values obtained 48 h after adding 100 mM KCl to reactions that contained ≥86 μM $d(TG_4)$ are similar to the 10 h values (Figure 4A, closed diamonds). However, the 39 μM $d(TG_4)$ assembly reactions probably do not reach equilibrium distributions at 48 h (Figure 4A, open diamonds). It is unclear how well equilibrated the 4 and 12 mM samples become after 48 h; however, the results suggest that the measured ellipticities are probably similar to kinetically asymtotic α_a values. The α_a determinations have approximate uncertainties of ±5%.

Equilibrium Quadruplex Assembly Isotherm. A plot of the α_a as a function of the logarithm of the total strand

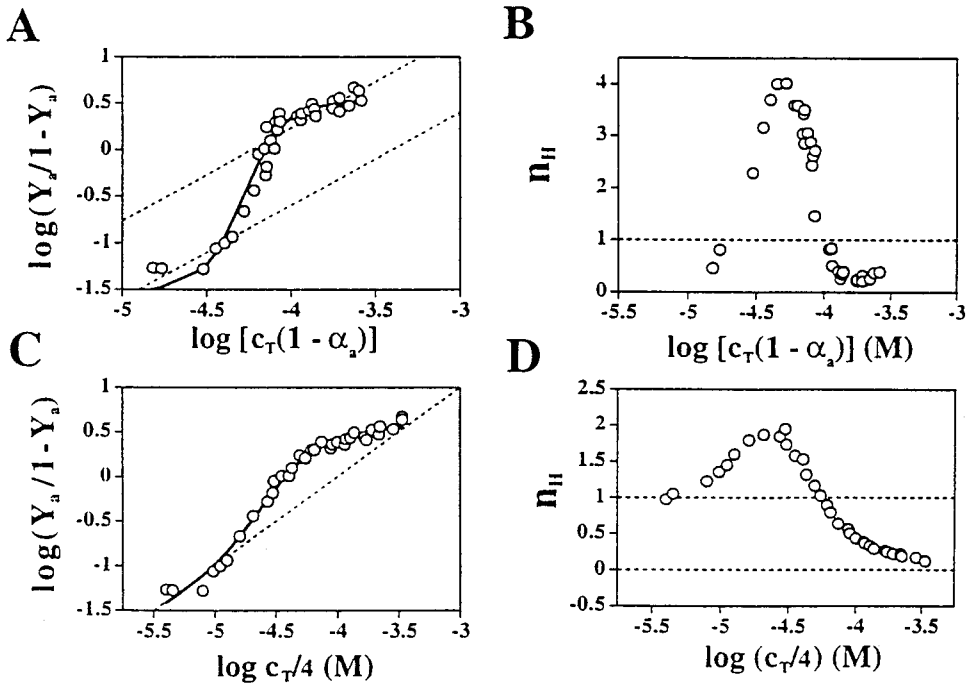

FIGURE 5: (A) Hill plot of the 48 h, 264 nm CD quadruplex assembly data (from Figure 5B) fitted to 3−, 4−, and 5−step Adair binding isotherms calculated using eq 8. Y_a is the fraction of assembled d(TG_4) strands. The diagonal line with a slope of unity represents results for a noncooperative process (aligned with the lower concentration data points). The 3- and 4-step fits nearly superimpose upon the 5-step fit. The 5-step model fits the data best based on visual comparison. Values were calculated assuming that intermediates species do not accumulate to appreciable extent, $S_{1,eq} = c_T(1 - \alpha_a)$. (B) The slope of the Hill plot (n_H) from panel A is plotted as a function of the initial d(TG_4) concentration. Cooperativity increases when the microscopic equilibrium constant increases ($K_i > K_{i-1}$) and the reaction becomes more spontaneous ($n_H > 1$); cooperativity decreases ($K_i < K_{i-1}$) at strand concentrations corresponding to $n_H < 1$. Slopes were calculated for consecutive pairs of points shown in panel A. (C and D) Same as panels A and B except assuming that $S_1 = 0.25c_T$.

concentration (log c_T) is shown in Figure 4B. Complete assembly occurs when α_a becomes 1. These results show that stability of the quadruplex increases dramatically at d(TG_4) concentrations around 10−20 μM and less so at higher $[d(TG_4)]_T$. This behavior is consistent with a high degree of positive cooperativity in the early stages of the quadruplex assembly reaction and negative cooperativity in the latter stages. The curve is not distributed sigmoidally about the mean ($\alpha_a = 0.5$), and data associated with α_a values ≥ 0.7 are spread across a significantly larger range of concentrations than at lower α_a, indicating that quadruplex assembly is suppressed in the latter stages. These observations suggest a quadruplex assembly reaction coordinate involving positive cooperativity, then negative cooperativity.

Association (binding) isotherms obtained upon equilibrating for 48 h at 37 °C are shown in Figure 4B. Given the relatively long equilibration period and stable limiting behavior, these results provide a reasonably good approximation of the equilibrium assembly isotherm.

The assembly data were analyzed on Hill plots to extract quantitative free energies and deduce the progression of cooperativity across the assembly reaction coordinate (Figure 5, panels A and C). The induced fit method of Cornish-Bowden and Koshland (1975) was chosen to fit the results to cooperativity profiles instead of the less flexible method of Monod, Wyman, and Changeux (MWC) (Changeux & Rubin, 1968; Wyman & Gill, 1990) because it includes both positive and negative cooperativity. To carry out the analysis, the magnitudes of the intrinsic microscopic (stepwise) equilibrium constants were varied to study the thermodynamic linkages between the subreactions in the quadruplex assembly pathway (Wyman & Gill, 1990).

Induced fit in the context of quadruplex formation can be inferred from the deviation of the slope of the Hill plot from unity (Figure 5, panels A and C). Binding data obtained after the 48 h incubation timepoint (Figure 4A, far right) were least-squares fit to eq 8 (Cornish-Bowden and Koshland, 1975) using two assumptions regarding the concentration of remaining ss at equilibrium: $S_1 = c_T(1 - \alpha_a)$ or $S_1 = c_T/4$ (see Methods). Adequate fits were obtained based on F-tests, nonsingularity of the Jacobian matrices and visual conformance to the data (see Methods). We tested models involving binding of three, four, and 5 strands to a presumed cation-bound, single-stranded "lattice". It was necessary to use four or five microscopic binding constants, K_i', to obtain sufficient flexibility to least-squares fit the data to reasonable conformance and capture the unique cooperativity pattern (Figure 6A). This implied the surprising result that complexes containing five and six strands participate in quadruplex assembly in addition to duplexes and triplexes. Arguments based on binding statistics (see Appendix) and results from concentration-jump kinetics analyses (manuscript in preparation) provide additional reasons to believe that this unexpected conclusion is correct. While a relatively wide range of possible solutions was screened, we did not attempt Monte Carlo (global) analysis of the problem, so additional reasonable fits might exist.

Two sources of confusion might be encountered below. (1) Two different models were used, the lattice-based "induced fit" (C-BK) model is different from the "lattice-independent strand aggregation" (LISA) model. (2) It might lead to confusion that either K^+ or strand ligands are assumed to bind a scaffold composed of an initial strand. The C-BK model is the same as used in their 1975 paper, but in the

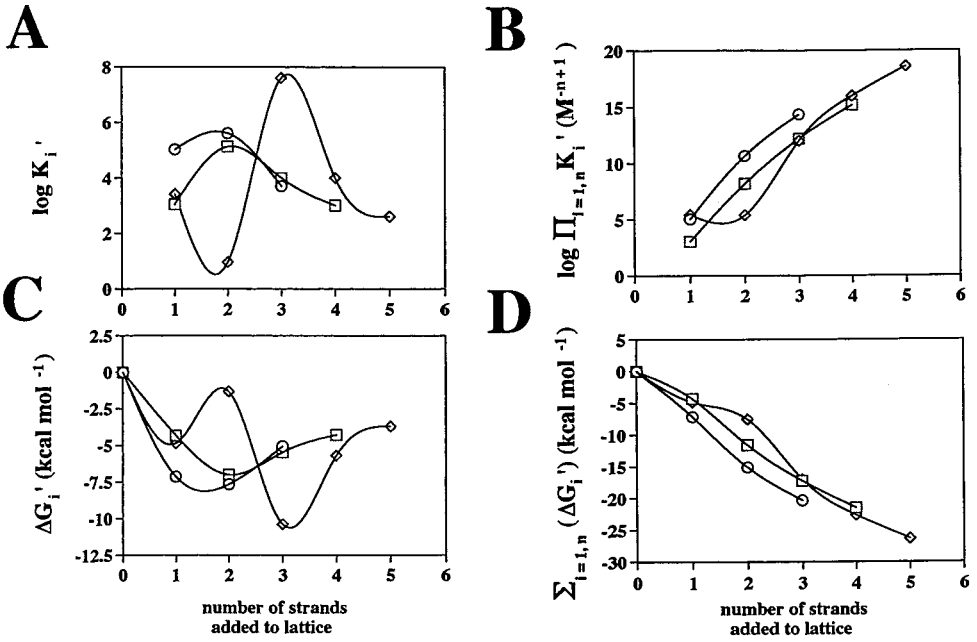

FIGURE 6: (A) Logarithms of "induced fit" microscopic quadruplex association constants (log K_i') obtained by nonlinear least-squares fits of the assembly isotherm assuming $S_1 = 0.25c_T$ (Figure 5C and D). Data are plotted as a function of number of strands added to the lattice as defined by eq 7 and fit for lattices binding either 3 (○), 4 (◇) or 5 (□) strands (Cornish-Bowden & Koshland, 1975). The lattice is assumed to be a [strand·cation] complex, implying that these modeled complexes have 4, 5, and 6 strands, respectively (see text). Interpolated lines are included to clarify the trends between points. (B) Logarithms of the products of K_i' are plotted as a function of number of strands added to the lattice using the results from panel A. (C) $\Delta G_i'$ calculated from the results in panel A. Interpolations were made between data points to clarify the trends. (D) Sums of the microscopic free energy contributions to quadruplex assembly correspond to net binding affinity of each strand addition subreaction (from panel C).

form of a general binomial distribution expression (eq 8), like that of Weber (1991). We include an explicit example for a [tetramer·(ligand)$_4$] binding lattice system (eq 9).

Our exact interpretation is that strands bind to a lattice which we assume to be an initial cation-bound strand. We maintain that the exercise is useful because it provides a first glimpse of the allosteric energies and progressive energy patterns that facilitate the early stages of assembly and inhibit the latter stages. The results are probably capturing significant features of the energetics, but there are complications regarding interpretations.

We used the C-BK approach with some reservation. The goal was to understand the energies of the subreactions in quadruplex assembly. The central questions are (1) does the reaction involve simple cooperativity or true allosterism and (2) does the C-BK model offer advantages relative to more conventional "linear aggregation" models [see Wyman and Gill (1989)]? We think the answers are (1) true allosterism and (2) it does. Definitions of "allosterism" vary and are somewhat disparate regarding details. Typical textbook definitions revolve around external (allosteric) effectors, which bind and thereby alter the activity of a *preformed* entity (*e.g.*, stepwise O_2 binding to hemoglobin tetramer). Broader definitions include effector-induced changes in aggregate subunit number (Wyman & Gill, 1989). Since previous linear aggregation models do not always explicitly stipulate distribution statistics (*e.g.*, binomial distributions are assumed in the C-BK model) or are more limited in application, we chose the well-established and versatile C-BK approach.

The "fractional saturation" index in the Hill plot, Y_a, is the extent of saturation of all of the binding sites on the "lattice" and was assumed to equal α_a (Figure 4). Plotting the ligand binding fraction $Y_a/(1 - Y_a)$ spreads the data out and emphasizes the d(TG$_4$) concentration range corresponding to $Y_a = 0.5$, the "switchover point" in the binding isotherm. This allows easier detection of changes in microscopic binding constants, and thus quantitative assessment of cooperativity.

Hill slopes (n_H), determined from the data as simple analytic (running two point) slopes, are plotted as a function of d(TG$_4$) concentration in Figure 5, panels B and D. When n_H is greater than one, the reaction is positively cooperative (*i.e.*, $K_{i+1}' > K_i'$). When $n_H < 1$, the reaction is negatively cooperative (*i.e.*, $K_{i+1}' < K_i'$). Positive cooperativity is observed for quadruplex assembly in the 5−50 μM d(TG$_4$) concentration range, where n_H is >1. Negative cooperativity is observed above 100 μM d(TG$_4$), where n_H is <1.

Expressions for lattice involving 2, 3, 4, and 5 sites were specified and incorporated into separate nonlinear least-squares fit programs in SAS then fit against the assembly data. Microscopic equilibrium constants K_i' for steps associated with addition of the listed number of strands to the lattice were derived from the fits (Tables 6 and 7) and are shown in Figures 6A and 7A. Products of the K_n' values are listed in Tables 6 and 7 and shown in Figures 6B and 7B to illustrate the net binding constant for all of the steps to a given point in the reaction coordinate. The dimensions of these products are (molarity)$^{-n+1}$ for n bound strands.

Products of equilibrium constants for all of the steps ($n = 5$), $\Pi_{i=1,5}K_i'$, are 3.8×10^{18} M^{-4} assuming $S_1 = 0.25c_T$ and 6×10^{13} M^{-4} assuming $S_1 = c_T(1 - \alpha_a)$. The quadruplex is very stable, especially after extrapolation to 23 °C (Table 2). This is in agreement with reciprocal dissociation constants determined by absorbance melt experiments. Note that the $\Pi_{i=1,n}K_i'$ values are not as large as the extrapolated reciprocal K_d values. This suggests that either the extrapolation is not reliable (*i.e.*, $\Delta C_p \neq 0$), different pathways predominate in the assembly and dissociation directions,

Table 6: Microscopic and Overall Association Constants Used To Fit the C-BK [$d(TG_4)_4 \cdot (K^+)_{3-5}$] Assembly Binding Isotherm and Strand Number−Dependent Association Free Energies

		Microscopic Equilibrium Constants (per strand bound)				
parameter[a]	n[a]	1	2	3	4	5
K_i' (unitless)	3	1.06×10^5	4.07×10^5	5.00×10^3		
	4	1.10×10^3	1.34×10^5	9.97×10^3	1.00×10^3	
	5	2.57×10^3	9.33	4.01×10^7	9.94×10^3	4.01×10^2
K_i'/K_{i-1}' [b]	3		0.26	81.4		
	4		121.8	0.074	0.100	
	5		0.0036	4.297×10^6	2.479×10^{-4}	0.0403
$\Pi_{i=1,i} K_i'$ [c]	3	1.06×10^5	4.31×10^{10} M^{-1}	2.16×10^{14} M^{-2}		
	4	1.10×10^3	1.47×10^8 M^{-1}	1.47×10^{12} M^{-2}	1.47×10^{15} M^{-3}	
	5	2.57×10^5	2.40×10^5 M^{-1}	9.62×10^{11} M^{-2}	9.56×10^{15} M^{-3}	3.83×10^{18} M^{-4}
		Microscopic Free Energies (per strand bound)				
$\Delta G_i'$ (kcal mol^{-1})	3	−7.13	−7.65	−5.04		
	4	−4.31	−6.99	−5.45	−4.26	
	5	−4.84	−1.32	−10.37	−5.67	−3.69
$\sum_{i=1,n} \Delta G_i'$ (kcal mol^{-1})[d]	3	−7.13	−15.09	−20.34		
	4	−4.31	−11.58	−17.25	−21.51	
	5	−4.84	−7.63	−17.00	−22.67	−26.36

[a] Binding sites filled per lattice. Index i refers to the specified step in a n-step Adair binding isotherm, corresponding to intrinsic equilibrium association constant (C-BK, 1975). Values were calculated assuming that 25% of the sample remains in the single strand pool, $S_{1,eq} = 0.25c_T$; T = 37 °C. [b] Ratio of Adair constants. A value of 1 corresponds to no cooperativity in the transformation from species $(i-1)$ to species i; values <1 denote negative cooperativity; values >1 denote positive cooperativity. [c] Products of microscopic association equilibrium constants. [d] Sums of microscopic association free energies.

Table 7: Microscopic and Overall Association Constants, Cooperativity Ratios, and Strand Number−Dependent Association Free Energies Used To Fit the C-BK [$d(TG_4)_4 \cdot (K^+)_{3-5}$] Assembly Binding Isotherm

parameter[a]	1	2	3	4	5
	Microscopic Equilibrium Constants (per strand bound, $n = 5$)				
K_i' (unitless)	3.32×10^3	7.5	1.49×10^7	2.75	59.09
K_i'/K_{i-1}' [b]		2.27×10^{-3}	1.99×10^6	1.85×10^{-7}	21.5
$\Pi_{i=1,n} K_i'$ [c]	3.32×10^3	2.49×10^4 M^{-1}	3.71×10^{11} M^{-2}	1.02×10^{12} M^{-3}	6.03×10^{13} M^{-4}
	Microscopic Free Energies (per strand bound, $n = 5$)				
$\Delta G_i'$ (kcal mol^{-1})	−5.00	−1.24	−10.17	−0.62	−2.51
$\Sigma_{i=1,n} \Delta G_i'$ (kcal mol^{-1})[c]	−5.00	−6.24	−16.41	−17.03	−19.54

[a] Calculated from the equilibrium binding isotherms by assuming that intermediates species do not accumulate to an appreciable extent, $S_{1,eq} = c_T(1 - \alpha_a)$; T = 37 °C. Two, three, and four strand addition models did not yield satisfactory fits. [b] Ratio of microscopic equilibrium constants defines the "cooperativity ratio". [c] Products of microscopic association equilibrium constants and sums of microscopic association free energies.

which produces hysteresis, or both factors are operative.

The corresponding free energies ($\Delta G_i'$) for the 3-, 4-, and 5-strand models are shown in Figure 6C. Sums of these values are listed in Tables 6 and 7 for each of these strand-addition reactions and shown in Figures 6D and 7D, respectively. These results express the energetic cooperativity profiles and net energies accrued at each stage in the assembly reaction quantitatively. The reactions all have negative free energies. The second steps in the 3- and 4-strand addition models are more favorable than the first; subsequent steps are less favorable. Said differently, binding of the first strand to the "lattice", results in more facile binding of the second strand. The energetic drive behind the third and fourth reactions becomes progressively smaller. Strand binding is positively cooperative in the initial two steps, then negatively cooperative in the latter steps.

Models which involve adding five strands to the lattice fit the data best under both equilibrium S_1 concentration assumptions [$S_1 = c_T(1 - \alpha_a)$ and $S_1 = 0.25c_T$)]. This was the only viable model when S_1 was set equal to $c_T(1 - \alpha_a)$ (Figure 7). Both calculations predict that triplex to quadruplex conversion makes the largest individual contribution to the net free energy change required to convert single strands to quadruplex (Figure 7, panels A and B). The cooperativity pattern is dominated much more by the free energy of the triplex to quadruplex transformation under the $S_1 = c_T(1 - \alpha_a)$ assumption. The other steps make relatively small contributions to the net free energy. In contrast, the 1- and 2-strand addition reactions contributed the largest individual free energies in the $S_1 = 0.25c_T$ model for $n = 3$ and 4 (Figure 6). Free energies required for duplex and quadruplex formation reactions (for $n = 3$) and pentaplex formation (for $n = 4$) were only slightly smaller. In contrast, for $n = 5$ assuming $S_1 = 0.25c_T$, triplex formation requires about 5-fold less energy than duplex formation and about 10-fold less energy than quadruplex formation (Figure 6). Since we do not have much knowledge regarding the extent of intermediate accumulation, we cannot place more emphasis on one of these models; however, we think they give some indication regarding the range of behaviors which might be expected with regard to cooperativity and numbers of strands involved in quadruplex assembly.

LISA Models for Quadruplex Assembly. A set of *lattice-independent strand aggregation* (LISA) models was also tested to fit the equilibrium assembly isotherms (Figure 8A). Derivation of expressions for Y_Q in the context of these models is discussed in the Appendix. These models were developed and tested because aggregation seemed to be a likely pathway for quadruplex formation. The C-BK approach is not specifically interpretable within the context of

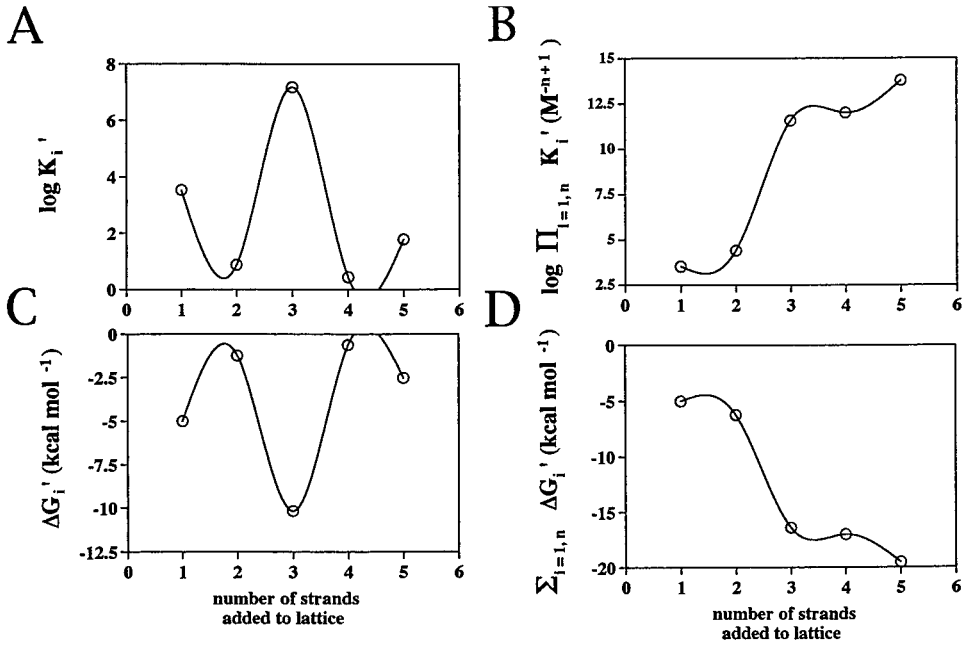

FIGURE 7: (A) log K_i' obtained by nonlinear least-squares fits of the assembly isotherm assuming $S_1 = c_T (1 - \alpha_a)$. Results analogous to (B) log ($\Pi_{i=1,n} K_i'$); (C) $\Delta G_i'$; and (D) $\Sigma_{i=1,n} \Delta G_i'$. Only the model for a lattice with five binding sites could be fit to the results. The three and four strand models were too stiff to provide satisfactory fits. Except for S_1, the assumptions and definitions are as in Figure 6.

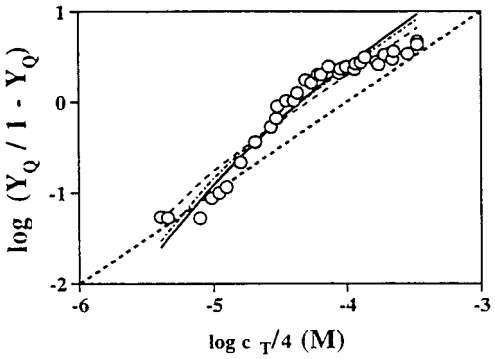

FIGURE 8: (A) Nonlinear least-squares fit LISA binding isotherms calculated using models involving duplex-duplex aggregation (—), and triplex-single-strand aggregation (-•-•-) (see Appendix). Y_Q is the fraction of strands that assemble into quadruplexes.

quadruplex assembly because the nature of the "lattice" is unclear. The LISA models explicitly define each bound component. The LISA models are defined with respect to the microscopic equilibrium constants in terms of *fraction of strands bound in quadruplex*, Y_Q, and not those that are bound to intermediate structures. If a reasonable fit can be obtained, they might provide a better defined assembly mechanism.

The change in ellipticity at 264 nm is ostensibly only due to quadruplex formation; however, contributions due to assembly intermediates also may contribute to these values. In the C-BK model (eq 8), Y_a is the *fraction of strands bound to the lattice*, which we interpret to be the first strand in an assembling quadruplex. Thus, all of the intermediates are included in Y_a and the model does not conform strictly to strands undergoing quadruplex formation alone, but rather to strands incorporated into all complexes. When reactants and intermediates are unfavored, $Y_a \approx Y_Q$.

Aggregation models for two different pathways were fit to the quadruplex assembly data. The first mechanism involved duplex, triplex and quadruplex formation by addition of three successive strands (Table 8; see Appendix). The second model involved duplex formation followed by dimerization of two duplexes to form the quadruplex. Since triplex formation is almost certainly easier than quadruplex formation, a third model was developed which includes acquisition of a single strand by duplex to form a triplex, but the triplex is not allowed to take on another stand to form a quadruplex. In a fourth model, quadruplex formation by strand addition to the triplex was allowed at the same time as duplex dimerization. This equilibrium scheme involves two simultaneous pathways which share the same reactants (duplexes) and products (quadruplex). The equilibrium involves bifurcation into two parallel pathways depending upon the preferred fate of duplex intermediates. A "gating factor" (γ) was implemented to determine the preference of stepwise strand addition relative to duplex dimerization in the least-squares fit ($\gamma = 0.5$ indicates equal preference).

None of the models provided particularly good fits to the data (Figure 8), but all showed weak conformance. A similar approach to that used to fit eq 8 that involved screening of a set of possible solutions was used and the same criteria were used to judge solutions. On the basis of visual inspection, these fits are clearly worse than those that were obtained with the induced fit approach (compare Figures 5 and 8). The results indicate that duplex dimerization is more likely than step-wise strand addition (Table 8; $\gamma = 0.38$).

Microscopic equilibrium constants K_i' determined from fits to the stepwise strand addition and duplex dimerization models are shown in Figure 9B. Free energies for the respective subreactions ($\Delta G_i'$) are shown for the same two models in Figure 9C. Despite relatively poor fits to the data, interesting cooperativity patterns were obtained. The free energy required to complete the initial step in duplex dimerization, duplex formation, was very large (13.2 kcal mol^{-1}), while quadruplex formation required much less free energy (2 kcal mol^{-1}). The first two strand additions (duplex and triplex formation) occured with negative cooperativity;

Table 8: Microscopic and Overall Association Constants and Free Energies Obtained from Fits to the Lattice-Independent Aggregation (LISA) Models for the [d(TG$_4$)$_4$·(K^+)$_{3-5}$] Quadruplex Assembly Isotherm[a]

		Microscopic Equilibrium Constants (per strand or duplex binding step)			
parameter	model[a]	1−2	2−3	3−4	2−4
K_i'	4_{22}	2.05×10^9			24 M^{-1}
	4_{31}	1.21×10^5	4.98×10^3	5.50×10^5	
	3_{21}, 4_{22}	9.96×10^3	6.18×10^3		7.70×10^3 M^{-1}
	4_{31}, 4_{22} ($\gamma = 0.38$)[b]	1.00×10^4	1.02×10^4	5.00×10^4	1.70×10^3
K_i/K_{i-1}[c]	4_{22}				1.17×10^{-8}
	4_{31}		−0.0412	110	
	3_{21}, 4_{22}		0.620		1.25
	4_{31}, 4_{22} ($\gamma = 0.38$)		1.02	4.90	0.034
$\Pi_{i=1,n}K_i'$[d]	4_{22}	2.05×10^9			4.92×10^{10} M^{-3}
	4_{31}	1.21×10^5	6.03×10^8 M^{-1}	3.31×10^{14} M^{-2}	
	3_{21}, 4_{22}	9.96×10^3	6.16×10^7 M^{-1}		4.74×10^{11} M^{-3}
	4_{31}, 4_{22} ($\gamma = 0.38$)	1.00×10^4	1.02×10^8 M^{-1}	5.10×10^{12} M^{-2}	8.67×10^{15} M^{-3}
		Microscopic Free Energies (per strand or duplex bound)			
$\Delta G_i'$ (kcal mol^{-1})	4_{22}	−13.2			−1.96
	4_{31}	−7.21	−5.24	−8.14	
	3_{21}, 4_{22}	−5.65	−5.38		−5.51
	4_{31}, 4_{22} ($\gamma = 0.38$)[b]	−5.67	−5.69	−6.66	−4.58
$\Sigma_{i=1,n}\Delta G_i'$	4_{22}	−13.2			−15.2
(kcal mol^{-1})[d]	4_{31}	−7.21	−12.5	−20.6	
	3_{21}, 4_{22}	−5.65	−11.1		−16.6
	4_{31}, 4_{22} ($\gamma = 0.38$)[b]	−5.64	−11.4	−18.0	−22.6

[a] Step in the specified binding isotherm, corresponding to the microscopic association equilibrium constant. Pathways involve the following steps (see Appendix): path 1 (4_{22}, duplex dimerization), 1 + 1 → 2, 2 + 2 → 4; path 2 (4_{31}, step-wise strand addition), 1 + 1 → 2, 2 + 1 → 3, 3+ 1 → 4; path 3 (3_{21}, 4_{22}, duplex dimerization plus triplex formation), 1 + 1 → 2, 2 + 1 → 3; 2 + 2 → 4; path 4 (4_{31}, 4_{22}), 1 + 1 → 2, 2 + 1 → 3, 2 + 2 → 4, 3 + 1 → 4 (4_{22} and 4_{31}−paths 1 and 2−operative). [b] Gating factor γ describing the preference for the $4_{21,\ 31}$ route over the 4_{22} route determined as an adjustable parameter in the fit. Duplex dimerization is thermodynamically about twice as likely as stepwise strand addition. Calculations used equilibrium isotherm values, which assumes that intermediate species do not accumulate to an appreciable extent, $S_{1,eq} = c_T(1 - \alpha_a)$. [c] Ratios of microscopic association constants. A ratio of 1 corresponds to no cooperativity in the $i - 1$ to i transformation; ratios < 1 correspond to negative cooperativity; ratios > 1 correspond to positive cooperativity. [d] Products of microscopic association constants and sums of stepwise association free energies.

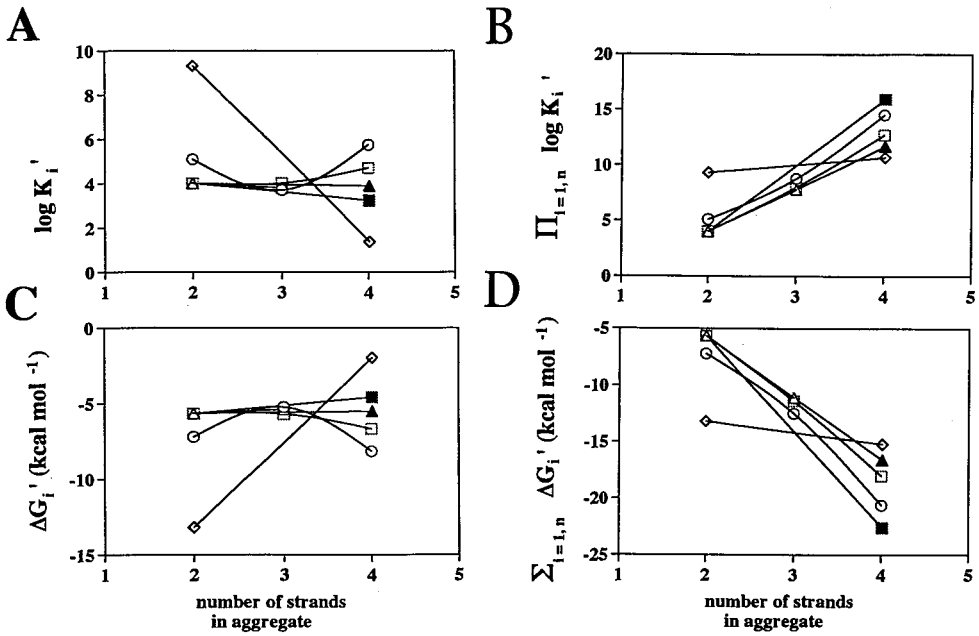

FIGURE 9: (A) log K_i' values calculated using the duplex dimerization (◇) and stepwise strand addition (○) aggregation models are plotted as a function of the number of strands in the aggregate. Interpolated lines between data points are shown to clarify the trends. Two separate paths can be taken by duplexes involving aggregation with either one or two strands as indicated by the bifurcating lines leading from the two-stranded species. Results were also calculated using mixed models involving (1) simultaneous triplex formation (□) and quadruplex formation by duplex dimerization (△), and (2) simultaneous quadruplex formation by both aggregation pathways (■, ▲). (C) Association free energies ($\Delta G_i'$) are shown as a function of strand number added in successive assembly steps. (D) Net $\Sigma_{i=1,n}\Delta G_i'$ values.

strand additions 2 and 3 (triplex then quadruplex formation) involved positive cooperativity. In contrast, the pattern obtained using the C-BK approach for $n = 3$ predicted positive cooperativity followed by negative cooperativity in the same three steps (compare Figures 9C and 6C). As expected, the mixed nonlattice models had intermediate behaviors relative to calculations with the isolated duplex dimerization and strand-addition models (Figure 9C).

DISCUSSION

Williamson (1994) concluded that the quadruplex to single strand dissociation equilibrium is not achieved until at least many minutes after setting the temperature during absorbance thermal denaturation analysis. The lack of rapid equilibration was confirmed for the 4 $d(TG_4)$ + 3−5 K^+ ↔ $[d(TG_4)_4 \cdot (K^+)_{3-5}]$ reaction using the absorbance thermal denaturation technique and circular dichroism assembly assay. To ensure measurement of equilibrium binding energies, the extent of reaction for quadruplex assembly was monitored as a function of elapsed time at 264 nm to determine the amount of time required for complete assembly to occur.

The necessity of doing these experiments was reinforced by results from CD relaxation experiments done to study the kinetics of $[d(TG_4)_4]$ formation (manuscript in preparation). Biphasic relaxation traces obtained using the CD band at 264 nm to monitor quadruplex formation indicate that $[d(TG_4)_4]$ assembly occurs either via two parallel pathways or in a reaction that requires two rate-limiting stages. Interpreting the relaxation data in mechanistic terms required knowledge of the equilibrium properties of quadruplex assembly (under the chosen conditions). The kinetics experiments were actually done first. However, attempts to analyze the results made it clear that equilibrium studies should be pursued, analogous to analyses of binding and linkage done with hemoglobin and its various allosteric effectors (Wyman & Gill, 1990). CD was used because the signal-to-noise ratio was much better than obtained in absorbance analyses.

Thermodynamic Evidence for Cooperativity in DNA Quadruplex Dissociation. The decreasing ordinate value in Figure 2 in the presence of 400 mM KCl (the differential thermal denaturation curve peak width) indicates that increasing the strand concentration increases positive cooperativity (synergistic interactions) between KCl and quadruplexes, even though it does not result in more dissociation. The 100 mM KCl samples do not show this synergism. At higher ionic strength, the temperature range which separates associated and dissociated states narrows, *i.e.*, the sigmoidal melt curve is sharper (Figure 2), even though the T_m increases. Said differently, dissociation is more cooperative at higher ionic strength even though the reaction doesn't go to products as easily (compare Figure 1A with Figure 2). Increasing the K^+ concentration from 100 to 400 mM results in a large increase in positive cooperativity at higher DNA concentrations. This occurs despite high K^+ to DNA phosphate ratios in both samples (>100:1). The transition state free energy barrier to assembly is large.

All of the melt samples contained >100-fold more K^+ than $d(TG_4)$ phosphates. The 100 and 400 mM KCl samples both contained 100 mM $Tris^+$, which has a pK_a of 8.1 and is over 90% protonated at pH 7. $Tris^+$ will compete more effectively with K^+ for phosphate binding when cations are almost equimolar than when K^+ is over 4-fold more concentrated. This suggests that $Tris^+/K^+$ competition produces the different cooperativity patterns found in 100 and 400 mM KCl. This implies that higher salt concentrations stabilize the transition state of the dissociation reaction more effectively than lower salt concentrations. The 400 mM KCl condition is thought to possibly encourage end-to-end complex−complex dimerization (manuscript in preparation). If so, the dissociation salt dependence results might be rationalized by a mechanism in which dissociation can proceed via the duplex-quadruplex reverse disproportionation route at 400 mM KCl (to produce two triplexes), but less so at lower ionic strength. Other mechanisms involving salt-stabilized transition states might provide alternative explanations for the increased cooperativity in quadruplex dissociation at 400 mM KCl relative to 100 mM KCl.

Guo *et al.* (1993) determined the thermodynamics for melting the same quadruplex we studied, $[d(TG_4)_4]$. Our measurements were done in 100 mM Tris-HCl (pH 7), 100 mM KCl, and employed 0.81 mM $d(TG_4)$; their samples contained 10 mM sodium phosphate (pH 7), 200 mM NaCl, 0.1 mM EDTA, and 0.1 mM strands. The results of these two studies are compared in pairs; keep in mind that these association propensities are inferred from dissociation constants: T_m, 69.3 [ours (o)], 61.2 °C [Guo *et al.* (1993) (G)]; ΔG°_a, −43.1 (o), −35.5 kcal mol^{-1} (G); ΔH°_a, −200.7 (o), −142.3 kcal mol^{-1} (G); and $-T\Delta S^\circ_a$, 157.6 (o), 106.8 kcal mol^{-1} (G). Their ΔG°_a produces an extrapolated K_a ($1/K_d$) at 25 °C of 1.09×10^{26} M^{-1}; our value was 6.4×10^{35} M^{-1}. These values are reasonable, considering the differences in strand concentration and ionic strength. Our higher strand concentration, cation (K^+ vs Na^+) and higher ionic strength should all favor more stabilization than observed by Guo *et al*.

Kinetics studies done as a function of ionic strength, cation type, Tris-HCl concentration and pH indicate that *100 mM Tris-HCl at pH 7 destabilizes quadruplexes by enhancing dissociation* (manuscript in preparation). Phosphate buffer is not as effective as $Tris^+$ in inducing duplex dissociation. Thus, 100 mM KCl and 100 mM Tris-HCl is expected to destabilize a quadruplex more effectively than the 10 mM sodium phosphate (pH 7) and 200 mM NaCl condition used by Guo *et al.* (1993). This suggests that our quadruplex might be even more stable than that of Guo *et al.* under the same conditions.

Guo *et al.* (1993) found that adding one 5′ adjacent T to get $d(T_2G_4)$ decreased the stability of the quadruplex by 1.3 kcal mol^{-1}; adding two 5′ terminal Ts (T_3G_4) reduced the stability of the resulting quadruplex by 8.5 kcal mol^{-1}; adding three Ts (T_4G_4) reduced it by 13.1 kcal mol^{-1}; adding seven Ts (T_8G_4) reduced it by 14.5 kcal mol^{-1}. This destabilization was attributed to tight stacking of the 5′-adjacent T base on the G residue in $d(TG_4)$ and progressive disordering of the less stack-prone Ts as the T tract length is increased.

The imino proton spectrum of $[d(TG_4)_4]$ in 10 mM sodium phosphate (pH 7) and 1 mM EDTA at 20 °C has four reasonably well resolved peaks (see Supporting Information). If the four strands are aligned in parallel, the spectrum should contain four peaks, due to four sets of four axially equivalent hydrogen atoms. The spectrum should contain eight peaks if there are two sets of antiparallel strands, due to 4 G imino protons per strand. Protons would be in four types of environments: abutted against the 5′-terminal Ts, internal (2 types) and 3′-terminal. The results are most consistent with the interpretation that the complex has four parallel-stranded G-quartets. The spectrum should be more complicated (dispersed) for the antiparallel quadruplex since at least twice as many imino proton environments should result.

Does $d(TG_4)$ form slipped DNA structures? In principle, an additional strand could bind to the vacated base-pairing sites of overhanging strands, and thereby form aggregates with five, six, or more total strands. This might occur readily

with $d(TG_4)$ strands, especially to form transiently slipped complexes. However, on the basis of results from statistical mechanical analyses, Hill (1986) concludes that the most stable structures should occur when the ends are flush. Overhanging ends disturb the surrounding water, resulting in unfavorable entropic contributions to the stabilization free energy. The overhang perturbs the degree of configurational order of surrounding solvent relative to solvent in the vicinity of flush-ended aggregates.

Xu *et al.* (1993) did absorbance and ^1H, ^{23}Na, and ^{39}K NMR melt analyses with the quadruplex formed by $d(T_2G_4T)$ in 18 mM NaCl at pH 7.4. Most of the imino proton peak intensity was lost due to buffer-induced exchange line broadening as the intact structure dissociated at >70 °C. Three small narrow peaks remained in the downfield region of the imino proton envelope when quadruplex hydrogens were exchanged with solvent hydrogens at elevated temperatures. The remaining hydrogen-bonded structure was christened the "open" form of quadruplex. Upon denaturation at 90 °C then cooling to 10 °C, Xu *et al.* (1993) found that only 60% of the strands reformed quadruplex. These investigators deduced that the "open" form is separated from the intact quadruplex by a large kinetic energy barrier.

Our NMR results for $[d(TG_4)_4]$ (see Supporting Information) suggest that the "open" $[d(T_2G_4T)_n]$ structure of Xu *et al.* (1993) might be a reasonably stable triplex dissociation intermediate, which may not be energetically predisposed to further dissociation under the experimental NMR melt conditions. In contrast with the four discrete imino peaks in the spectrum of $[d(T_2G_4T)_4]$ (Xu et al., 1993), a single exchange-broadened peak was observed during all stages of thermal denaturation, in 1, 10, and 100 mM Tris-HCl (pH 7), in both 10 and 100 mM KCl (manuscript in preparation). This implies that $[d(TG_4)_4]$ can cross the dissociation-association transition-state barrier more efficiently than $[d(T_2G_4T)_4]$. This suggests that less triplex should accumulate during denaturation of $[d(TG_4)_4]$ than with $[d(T_2G_4T)_4]$ because $[d(TG_4)_3]$ triplex is converted to quadruplex more efficiently than $[d(T_2G_4T)_3]$.

The DNA concentrations used in our absorbance melt studies were at least 10-fold more dilute than used by Xu *et al.* (1993) in their NMR experiments. A slowly dissociating triplex intermediate might be sufficiently long lived at their high DNA concentrations to allow observation of discrete, slowly exchanging $[d(T_2G_4T)_3]$ triplex imino peaks. A higher total strand concentration should act to suppress further dissociation. Mass action should drive the dissociated components to reestablish equilibrium after mixing with K^+ by forming stable complexes other than quadruplexes. Cation-deficient strand concentrations should decrease when KCl is added due to the following reactions: $R_1 + m\,K^+ \rightarrow T_1$ and $T_1 + R_{n-1} \rightarrow T_n$. R refers to *relaxed*, cation-deficient strands; T refers to *tense*, cation-saturated strands. Duplexes (R_2, T_2) and triplexes (R_3, T_3) accumulate as R_1 and T_1 pools are depleted. When the R_1 concentration decreases, intermolecular collisions occur less often between uncomplexed strands and duplexes, and more often between two- and three-stranded complexes. Potassium acts as an allosteric effector by driving R_n complexes (and strands) to form T_n (and $T_{n+1,\ldots}$) complexes. The result is that the average number of strands per complex increases.

Removing cations drives dissociation reactions. Importantly, once quadruplexes form, they are very stable and must cross a large transition state free energy barrier to dissociate. Strand and/or cation concentrations can be reduced considerably, yet the complex can remain primarily intact, in a metastable state.

Anything that can "seep into" the hydrogen-bonded and salt-bridged interstitial spaces between strands of predominantly intact quadruplexes, via either the sides or the ends, and displace strands from each other, will lower the dissociation free energy barrier. This suggests a general conceptual model for how quadruplex dissociation could be induced by environmental effectors, including small molecules, proteins, or even other nucleic acids.

Low to intermediate cation concentrations lead to structural diversification, increased assembly intermediate concentrations, and more frequent intercomplex encounters. At high cation concentrations, intercomplex interactions would be more shielded and the Donnan spheres of cations surrounding the anionic complexes would probably lead to fewer encounters (manuscript in preparation). At some intermediate concentration, we think cations might act like a contact- and lateral movement-promoting medium which is conducive to slippage and might even help mediate strand transfer between complexes. By analogy, motorcycle chain lube both lubricates and facilitates the grip between the chain and gear. Nuclear and cellular homeostasis might be especially well tuned to optimize this tendency or under some circumstances minimize it. DNA sequences may be under selective pressure to benefit from or prevent misfunctions due to strand−strand intermingling. Since such interactions might well lead to increased recombination frequencies, this phenomenon may promote interchromosomal translocation events, possibly leading to cancer or other genetic diseases (Hardin *et al.*, 1993; Fearon & Vogelstein, 1990).

Cation Depletion and "Pseudocooperativity". How much does the free cation concentration differ from the total cation concentration? Cations are either condensed around the polyanionic quadruplex, bound internally within the complex, or unbound. If a substrate must bind a metal to participate in an enzymatic reaction, a sigmoidal activity versus concentration curve is observed when metal−substrate (reactant) complex formation is inhibited, since insufficient viable reactant is produced. At low metal concentration, little viable substrate accumulates unless the K_a for [cation·enzymatic substrate] complex formation is large. For example, human brain hexokinase shows "pseudocooperative" activity curves at submillimolar Mg^{2+} concentrations because the cation is required for conversion of presubstrate ATP^{4-} to activated substrate $[Mg{\cdot}ATP]^{2-}$, which has a much lower Michaelis−Menten constant in the enzymatic reaction with hexose (Fromm, 1975). Viable substrate formation is limited by the low K_a for Mg^{2+} with ATP^{4-} (*ca.* 10^6 M^{-1}), which leads to sigmoidicity in the activity curve at low $[Mg^{2+}]$.

The amount of K^+ available to drive quadruplex assembly depends on the total K^+ concentration, the K_a of the K^+ aquo complex (Ross & Hardin, 1994), and the K_a of the cation with other competing ligands, especially $d(TG_4)$ phosphodiester phosphates. The depletion in bulk K^+ concentration due to counterion condensation can be calculated if one knows the average occupancies of cation at each phosphate in the quadruplex and single-stranded species, and any significantly populated intermediates present at equilibrium. Following Xu *et al.* (1993), we estimate that each phosphate in the

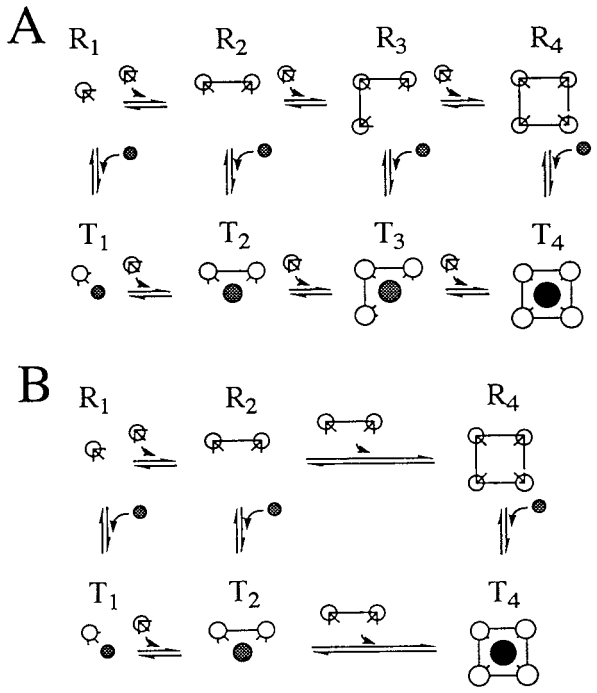

FIGURE 10: (A) Stepwise strand addition and (B) duplex dimerization quadruplex assembly reactions. Relaxed (R) to tense (T) transitions are driven by K^+. Deactivated R_n form strands are shown as smaller white spheres. Strands acquire an increased propensity to form quadruplex by binding cations, which converts complexes to the T_n and $T_{n+1,...}$ forms. Cation-bound strands are shown as larger white spheres. Activated cations are symbolized by grey spheres with radii that increase as one progresses across the parallel R and T assembly pathways. Relaxed and tense structures 2−4 are interconnected by hydrogen bonds (horizontal and vertical lines). Transformations to T structures are encouraged by strand-cation salt bridge formation, which increases the density of interconnectivities between strands, and between stands and cations. The propensity for additional strands decreases as strands are added to form larger complexes. Cation-bound single strands (T_1) are more tense than T_2, T_3, and T_4 species. Quadruplex have a low propensity for strands, making them less tense than (in the following order) triplexes, duplexes, and single strands.

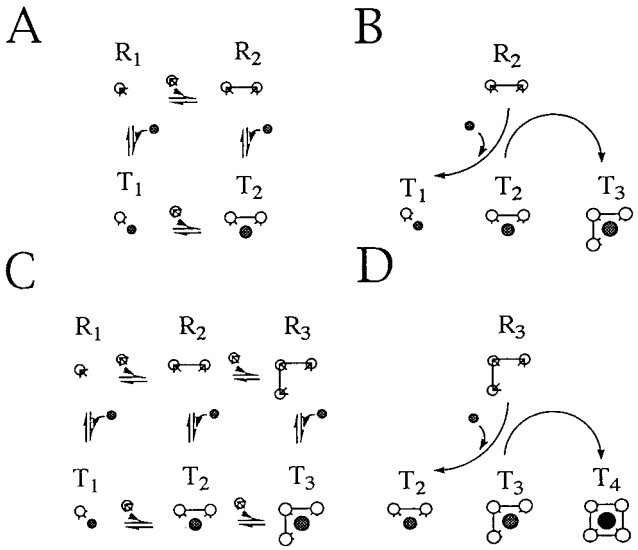

FIGURE 11: (A) Strand addition subreactions leading to R and T form (A) duplex and (C) triplex precursors required for disproportionation reactions in which (B) two duplexes and (D) two triplexes produce a triplex and a single strand, and a quadruplex and a duplex, respectively. Symbols are as defined in Figure 10.

quadruplex is fully neutralized by cation. Since α_a values were $< \sim 85\%$, we assume that the remaining strands were present as single strands, with occupancies of 0.68−0.71 cation per phosphate (Record *et al.*, 1976). If we also assume that one cation is bound at the 3′-terminal end of the quadruplexes, we calculate that at most *ca.* 2% of the total 100 mM KCl present in the association reaction samples is bound. Duplexes and triplexes should have cation-phosphate occupancies of 0.88−0.93. The error in our estimates introduced by intermediates is probably small. Since K^+ is present in at least 50-fold excess over possible quadruplex formed and K_a values for externally bound cations are probably $\leq 10^3$ M^{-2} (Xu *et al.*, 1993), we conclude that "pseudocooperativity" probably does not contribute substantially to the sigmoidicity found in the quadruplex association isotherms.

Allosteric Profile of the Association Reaction. Quadruplex formation is a complex process consisting of up to 10 linked equilibria (Figures 10 and 11). To study such reactions, specifically their energies and cooperativity in the reaction coordinate, especially under conditions where concerted interactions are important, Adair developed the progenitor to the concept of "induced fit" substrate binding. Koshland and co-workers (Koshland *et al.*, 1966; Cornish-Bowden and Koshland, 1970, 1975) constructed analytic expressions to describe the relations between intersubunit geometries and predicted relative contributions of individual assembly step energies to the net observed energy.

The Adair−Koshland "induced fit" (AK) model is more flexible than the commonly applied MWC model (Changeux & Rubin, 1968), which does not include negative cooperativity in binding processes. The induction energy associated with the "induced fit" model is required to prepare the binding site for complex formation. Properties of the the Adair equation were illustrated in terms of the range of behaviors observed in Hill binding isotherms with different cooperativity profiles by Cornish-Bowden and Koshland (1975). Our quadruplex association results (Figures 6 and 7) fit a predicted plot in which positive cooperativity occurs in the early stages then gives way to negative cooperativity in the intermediate and final reaction steps. Strand addition occurs with some difficulty at first then becomes progressively less driven as complexes form and strands are removed from the reactant pool. Different detailed patterns result depending upon whether one assumes that significant amounts of intermediate species remain (Figures 5, panels C D, and 6) or are completely resolved into ss and Q pools upon equilibration (Figure 5A, 5B and 7).

Calculated Adair constants (K_i') were normalized by taking into account statistical factors which arise from the number of different ways *n* ligands can be distributed over the number of binding sites (see Appendix). The product of these microscopic binding constants is the apparent macroscopic association constant (Figures 6 and 7; Tables 6 and 7). In the case of the Adair−Koshland isotherm, these factors are predicted assuming a binomial distribution of *n*-stranded complexes. As a result of this normalization, Adair constants correspond to *intrinsic free energy changes* ($\Delta G_i'$) as a function of strand number added across the reaction coordinate. If properly applied, this analysis can in principle divulge the stepwise energetics associated with formation of specific linkages. The sum of the microscopic free energies is the net apparent assembly free energy. The 5-strand AK model gives an overall association constant

product ($\Pi_{i=1,n}K_i'$) of 3.8×10^{18} M^{-4} for corresponding to a free energy sum ($\sum_{i=1,n}\Delta G_i'$) of -26.4 kcal mol^{-1} (Table 6). This is in contrast to the extrapolated overall K_d at 23 °C of 1.6×10^{-32} M (inferred $K_a = 6.4 \times 10^{31}$ M^{-1}) under similar conditions (Table 2; $c_T = 0.81$ mM). Assembly and dissociation appear to be hysteretic processes and fail to achieve complete equilibration in the melt measurements (Wyatt *et al.*, 1996; Hud *et al.*, 1996). Some or all of the difference between $\Pi_{i=1,n}K_i'$ and $1/K_d$ may be the result of a temperature-dependent change in C_p, which would lead to error in the extrapolation of K_d from the T_m to 23 °C.

In the AK formalism, the lattice is bound by one or more substrates and allosteric effectors. We interpret the AK model in the quadruplex assembly situation as implying that an initial strand, and most likely a cation-neutralized strand, operates in the role of lattice. The lattice-nucleated AK model is less intuitively accurate than the strand aggregation (nonlattice) model because the second (binding) strand is distinguished from the first strand (lattice) in its role as a ligand. These considerations lead to the idea that more cation-saturated T_1 and T_n complexes act as recipient lattices for cation-deficient R_1 ligand strands. This makes it complicated to assess the total lattice concentration without information about assembly intermediate concentrations because the lattice concentration changes as ligand strands are absorbed into or released from the lattice strand complexes. This is unlike the typical situation in which a known amount of nontransmutable lattice is present and one has unequivocal knowledge regarding the lattice concentration (Wyman & Gill, 1990). The AK model provided well-determined fits to the quadruplex assembly data, yet the full underlying meaning of the results is still open to question.

A reasonable interpretation is that duplex formation occurs rather efficiently, followed by triplex formation, and that both reactions are more efficient than quadruplex formation. *A decrease in assembly efficiency should occur for each strand addition*. Each strand increases the net negative charge of the complex and, because the complex remains approximately the same length, increases its effective charge density. Since strands are anionic, they will increase the charge density of the lattice as they bind and thereby produce a progressively lower affinity for additional strands. While strand addition increases the lengths of the two shorter lateral axes, the effective hydrodynamic radius is determined primarily by rotation about the long axis, which is of similar length in duplexes, triplexes, and quadruplexes if they are all flush ended, or all have similar overhangs. Most of the phosphate charges are neutralized by atmospherically bound (condensed) cations; however, the net charge density of the complex will still increase.

Two results discussed by Singleton and Dervan (1993) support the contention that triplexes are more anionic than duplexes and single strands, but that the change in charge density decreases with strand number added. Neutralizing polymeric DNA and RNA duplexes with spermine leads to dismutation (disproportionation) to produce triplexes and single strands at neutral pH (Glaser & Gabbay, 1968). Morgan *et al*. (1986) found that spermine bound duplexes with 10-fold higher affinity than single strands but bound triplexes only 1.5-fold more strongly than duplexes.

Entropic Contributions to Association. Considering entropic factors, one might surmise that quadruplex disproportionation would be allowed in addition to a pathway involving condensation of one lone strand with a triplex or of two duplexes to form a quadruplex. A single strand has many more degrees of freedom than a strand that is constrained within a three-stranded complex. Every time a strand is incorporated into a quadruplex, a less constrained duplex is concurrently produced from the donor triplex. The net entropic free energy is approximately unchanged. However, each triplex formation step costs the constraint free energy required to incorporate a strand and duplex into a triplex (unless triplex can be produced by disproportionation of two duplexes). To illustrate, let's assume that duplex, triplex, Q, etc., lose 1 "freedom unit" (fu) in a binding reaction. In duplex formation, the loss of freedom is equal to the loss of two single strands in the reaction $S_1 + S_1 \rightarrow S_2$, plus the gain by the duplex, which we assume to be $+1$ fu. The net loss is $-2 + 1 = -1$ fu. A "lattice" could be defined crudely in terms of the *entropy content (loss of freedom) of a strand which is bound by a strand that loses its freedom*. The lattice strand also loses freedom, but a strand on a duplex is much less constrained (ordered and connected) than it would be if bound to a larger lattice. On a per triplex used basis, disproportionation is more costly than step-wise strand addition (-4 vs -3 fu). However, reformation of a duplex avoids another duplex formation reaction, so the net gain is $+1$ fu and disproportionation is equally likely to occur. Entropy-driven cycling would be expected to select the triplex-triplex and triplex-duplex pathways as frequently as the triplex-single strand condensation route. As a result, at *higher* single strand concentrations, the triplex-strand binding mechanism would be preferred, while at *lower* [ss] and higher [duplex] and [triplex], disproportionation might be expected to occur, or even predominate.

Guanine Stacking Is a Necessary Prerequisite for Efficient Assembly. Contiguous stacking of guanines and of the phosphodiester backbone is an obvious prerequisite to quadruplex formation. Relaxation results have been interpreted as providing evidence for stacking as a required pre-equilibrium step in DNA duplex formation (Williams *et al.*, 1989). The CD results shown in Figure 3B for the melted quadruplex species show that $d(TG_4)$ undergoes a rapid reversible transition from stacked to unstacked as the temperature is raised [also see Davis and Tinoco (1968) and Vesnaver and Breslauer (1991)]. The low-temperature form is competent to undergo quadruplex formation, while the high-temperature form is less stacked and presumably much less capable of incorporation into the quadruplex formation pathway. This pre-equilibrium can be incorporated into the quadruplex formation pathway as shown in Scheme 1. This is presumably why assembly kinetics are faster at lower temperature and slower at elevated temperatures. In contrast, rates of Boltzmann (B) energy-driven processes are typically proportional to k_BT, and therefore faster at higher temperatures.

In the Wetmur−Davidson−Manning model (Williams *et al.*, 1989), bases on strands line up to form a single-stranded (duplex-) assembly intermediate. This aligned strand is thought to acquire condensed counterions prior to (or in concert with) duplex formation. Applying this idea to quadruplex formation, we postulate that at low to moderate DNA and K^+ concentrations, strands cannot aggregate efficiently as a result of large anionic strand-strand repulsion energies, yet cations can condense around individual strands and base alignment can occur. High-strand association

Scheme 1: Early Stages in Quadruplex Formation

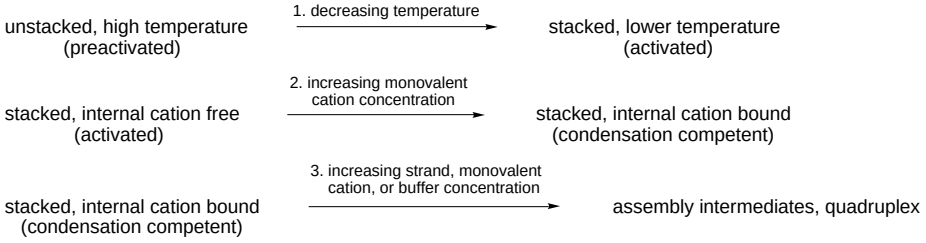

transition state barriers prevent Q formation, but assembly primed [stacked ss·(cation)$_n$] intermediates ($n_{stacked} > n_{unstacked}$) can form in large amounts. If cations (especially K^+ and Na^+) can bind in the interior groove, they can presumably nucleate strand aggregation events and thereby assist strands across the otherwise inhibitory assembly kinetic barriers (Scheme 1).

Most known telomeric DNAs are composed of a G-rich 3′-terminal end that overhangs complementary C-rich 5′ strand by approximately 12−16 nucleotides. Henderson and Blackburn (1989) showed that this G-rich overhang is a common characteristic of telomeres. Putative roles include forming at least three different types of quadruplex structures which function in chromosome protection, interchromosomal crosslinking, and recombination (Hardin *et al*., 1991; Venczel & Sen, 1996). Potential functions of monoatomic cations in driving transformations between such structures have received particular attention.

These G-rich telomeric overhangs may function as "antennas", which detect ionic conditions that are conducive to strand stacking and quadruplex assembly (Scheme 1). The strand could be used to sense appropriate changes in physiological conditions within the nucleus. These changes might be induced by signaling pathways via cation ports, and could conceivably set off a cascade of responses. For example, at low potassium, the G-rich strand from *Oxytricha* telomeres was found in X-ray studies to be gripped in its (preactivated) unstacked form within the binding site of the *Oxytricha* β protein (Schultz *et al.*, 1997). The protein separates the Gs in the DNA strand when bound within the binding site using intercalative aromatic side chains and histidine as ligands. This resembles the binding mode of single-stranded binding proteins such as the gene 32 protein from phage T4. When K^+ concentrations increase to levels high enough to offset the charge−charge interactions, the strands should release from the protein. In response, the bases might then stack, making the strands competent to interact with the β protein in another of its activities, chaperoning quadruplex formation (Fang & Cech, 1993a,b).

Telomeric sequences and G-rich transcriptional promoters have undergone intense scrutiny as targets for antisense genetic therapy. G-rich promoters are common targets for antisense growth control strategies, which work in some cases, but suffer from a number of poorly understood difficulties related to "position effects" which depend upon the structural context of the integrated transgene construct. More than 85% of human promoters are GC-rich (Bernardi, 1989). Promising antisense G-rich oligonucleotides might easily aggregate *in vitro* or *in vivo* to form undeliverable, and therefore undesirable, dead-end quadruplex complexes (Hardin et al., 1992; Olivas & Maher, 1995; Kandimalla & Agrawal, 1995; Deng & Braunlin, 1995; Miura et al., 1995). Strand and cation concentrations would determine how much DNA has antisense activity and the amount of DNA that accumulates as quadruplex and is thereby inactivated with respect to antisense activity. Knowing how to control the degree of strand partitioning into active and inactive pools requires knowledge about the effects of cation and strand concentrations on the extent of quadruplex formation. Such reactions might be used *in vivo* as a way to control the functional dosage of genetic elements (Kauffman, 1993).

ACKNOWLEDGMENT

We thank Charles Goss and Bill Ross for encouraging these studies and providing helpful editorial suggestions, and the reviewers for useful criticisms.

APPENDIX: LATTICE-INDEPENDENT QUADRUPLEX ASSEMBLY THERMODYNAMICS

Three *lattice-independent strand aggregation* (LISA) mechanisms were investigated. Methods developed by Cornish-Bowden and Koshland (1975) to analyze cooperative binding between enzymes with multiple binding sites and substrates were adapted to describe quadruplex aggregation. In the set of aggregation mechanisms that lead to quadruplex formation, duplex and triplex lattices are composed of single strand ligands. Strands act as both the *ligands* (*substrates*) that were envisioned by C-BK, and, when assembled, as the *lattice*. Unlike a monomeric protein that binds multiple substrates, the lattice can expand by binding additional *strands* (*ligands* and *subunits*).

Here, we show that C-BK methods are sufficiently general to permit extension to aggregation mechanisms. The common starting point is the definition of *fractional saturation* (Y), which we denote by Y_Q in the LISA models and define as the ratio of strands (ligands) bound in quadruplexes to total strands in the solution. This definition is similar to, but not the same as that of C-BK, *i.e.*, the ratio of bound ligand to total ligand, which we call Y_a, referring to all bound ligand, including those bound in quadruplexes, duplexes, triplexes, hexaplexes, etc. Using either definition of Y, the analysis proceeds by defining the quantity $Y/(1 - Y)$ in terms of component concentrations, then replacing component concentrations by the associated equilibrium constants, and finally determining equilibrium constants by fitting the expression to experimental data obtained from quadruplex assembly experiments.

We could have carried out the analysis and curve fitting just as well by defining Y as C-BK did, but we felt that our definition was a more direct reflection of our experiments in which we directly measure total strand concentration and quadruplex concentration.

We also show how we adapted the C-BK method for relating the apparent, macroscopic equilibrium constants to

the intrinsic, microscopic constants by examining the relative probabilities of adding or losing a strand for each possible configuration. Mechanistic considerations are presented more explicitly as schematics in the last section.

S_i	concentration of an *i*-plex (an aggregate consisting of *i* strands)
S_T	total single-strand concentration, $\sum_i S_i$
Y_Q	fractional saturation of quadruplex, the fraction of total strands (S_T) incorporated into quadruplex
$Y_Q/(1 - Y_Q)$	ligand binding fraction, the ratio of the number of strands incorporated into quadruplex to the number of strands not in quadruplex (the sum of all strands in the forms of single strand, duplex, and triplex): $Y_Q/(1 - Y_Q) = 4S_4/(S_1 + 2S_2 + 3S_3)$ (A1)
$\alpha_i, \beta_i, \gamma_i$	gating factors for multiple contributions to an *i*-plex
$K_{ij,k}$	*apparent* macroscopic equilibrium association constants for the reactions: $S_i + S_j \leftrightarrow S_k \quad (k = i + j)$ (A2)
$K'_{ij,k}$	*intrinsic* microscopic equilibrium constants for individual binding events
k_i, k_{-i}	apparent macroscopic forward and reverse association rate constants for the eq A2 reactions
k'_i, k'_{-i}	intrinsic microscopic forward and reverse rate constants for an individual binding event

Intrinsic (Microscopic) and Apparent (Macroscopic) Equilibrium Constants. Intrinsic equilibrium constants $K'_{ij,k}$ refer to a binding reaction between a specific binding site (or dual site for duplex-duplex binding) and an appropriate ligand. The *apparent* (measured) *equilibrium constant* $K_{ij,k}$ for the reaction $S_i + S_j \leftrightarrow S_k$ will not be equal to $K'_{ij,k}$ if there is more than one binding site, even if all the binding sites are equivalent and noninteracting.

Consider the set of subreactions involved in the formation of an *n*-plex by successive addition of a single strand. Addition of single strands is used to simplify the illustration; the results will be seen to apply to the more general form of subreactions between an *i*-plex and a *j*-plex when *j* is not equal to 1

$$S_1 + S_1 \leftrightarrow S_2 \tag{A3}$$

$$S_2 + S_1 \leftrightarrow S_3$$

$$S_{n-1} + S_1 \leftrightarrow S_n$$

By mass action, we associate an apparent equilibrium constant,

$$K_{(i-1)1,i} = [S_i]/[S_1][S_{i-1}] \tag{A4}$$

with the strand addition subreaction:

$$S_{i-1} + S_1 \leftrightarrow S_i$$

where ij,k is equal to $(i-1)1,i$ when the $i-1$ complex binds 1 strand to form the *i* complex.

The rate of change of $[S_{i-1}]$ is

$$d[S_{i-1}]/dt = -k_{i-1}[S_{i-1}][S_1] + k_{-i}S_i \tag{A5}$$

At equilibrium, $d[S_{i-1}]/dt = 0$ and we obtain the relation between the apparent equilibrium constant $K_{(i-1)1,i}$ and the apparent forward and reverse rate constants k_i and k_{-i} of this subreaction:

$$K_{(i-1)1,i} = k_i/k_{-i} \tag{A6}$$

First, consider the simple case of a substrate S with one binding site and a ligand L which together form a complex S·L through the reaction.

$$S + L \leftrightarrow S{\cdot}L$$

Here, $n = 1$, and there is no distinction between apparent and the intrinsic constants, so we can write

$$K = k'_1/k'_{-1}$$

where the intrinsic forward rate constant k'_1 is proportional to the probability that associations will occur during a collision between the ligand and the substrate binding site. Similarly, k'_{-1} is proportional to the probability of dissociation occurring during a collision between solvent molecules and an occupied binding site.

Now consider a similar substrate but with *n* equivalent noninteracting binding sites, of which $i - 1$ are occupied. The apparent probability that an association reaction will occur will be equal to the intrinsic association probability for the single site case, multiplied by the number of vacant binding sites before the association reaction, which is $n - i + 1$. Thus, the probability that an association reaction will occur is proportional to $(n - i + 1)k'_i$. The probability of a dissociation reaction is equal to the intrinsic dissociation probability for the single site case multiplied by the number of filled binding sites after the association reaction, which is *i*. Thus, the apparent equilibrium constant will be

$$K_i = (n - i + 1)k'_i/ik'_{-i} = [(n - i + 1)/i]K'_i$$

The "statistical factor", $(n - i + 1)/i$, in expression A6 relates the apparent equilibrium constants to the intrinsic equilibrium constants. This expression is in agreement with the result calculated from eqs 15−20, p 854, Cantor and Schimmel (1980). Note that Cantor and Schimmel refer to dissociation equilibrium constants while we refer to association equilibrium constants, they use the symbol *k* for the single microscopic equilibrium constants for all sites while we use K_i for addition of the *i*th strand, and they use $\Omega_{n,i}$ to indicate the number of distinct ways to put *i* ligands into *n* sites.

$$\begin{aligned} K_i &= (\Omega_{n,n-i}/\Omega_{n,i})k \\ &= \{n!/[(n - i + 1)!(i - 1)!]\}\{[(n - i)!i!]/n!\}k \\ &= \{i(n - i)!/[n - (i - 1)]!\}k \\ &= [i/(n - i + 1)]k \end{aligned}$$

Thus, for the case of equivalent, noninteracting binding sites, the general expression for the statistical factor that relates the apparent and intrinsic equilibrium constants of a subreaction is the ratio of the number of vacant binding sites before the reaction to the number of filled binding sites after the reaction. This formula may be applied to the more general form of subreactions between an *i*-plex and a *j*-plex when neither *i* nor *j* is equal to 1, by substituting the model of a multisite binding complex for the simple binding site.

To adapt this analysis to a nonlattice model, we interpret "number of vacant binding sites before the reaction" as "number of ways in which an *i*-plex and a *j*-plex can

Scheme 2: LISA Models

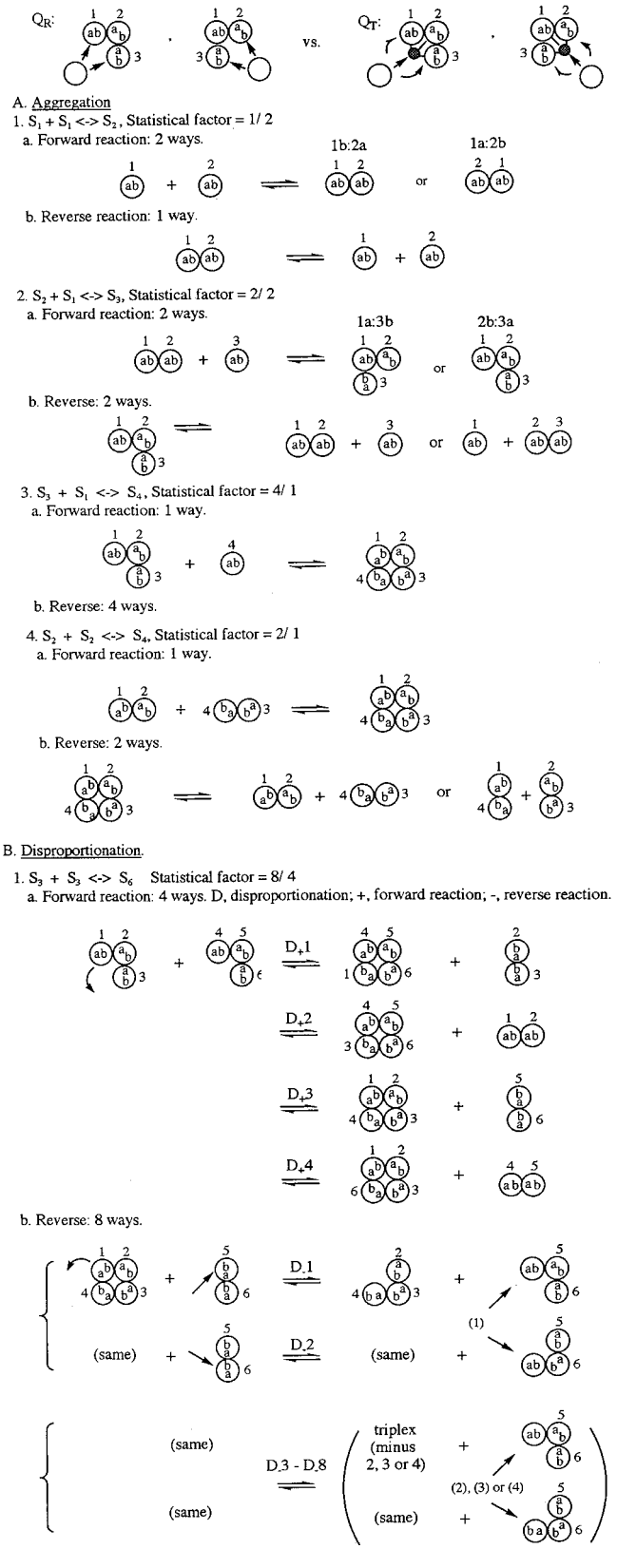

assemble", and we interpret "number of filled binding sites" as "the number of ways in which an $(i + j)$-plex can dissociate".

Statistical Factors for Nonlattice DNA Quadruplex Assembly Reactions. It is assumed that each strand has two different binding sites, a and b, and that only a and b sites can interact to form a junction. Only a−b interactions are considered because Gs have two hydrogen-bonding interfaces in G-quartets. We also assume that two strands are singly bound to the third strand, which is doubly bound. This is reasonable for the R-form triplex, but is less like the case of singly bound strands in T-form triplexes, in which cations serve to attach the third strand to a lattice involving the indirectly attached strand, intervening strand and cation (Scheme 2).

Assembly Mechanisms: 1. Stepwise Strand Addition in Terms of All Species Formed. The subreactions are

$$(1)\ S_1 + S_1 \leftrightarrow S_2$$

$$(2)\ S_1 + S_2 \leftrightarrow S_3$$

$$(3)\ S_1 + S_3 \leftrightarrow S_4$$

The apparent equilibrium constants are

$K_{11,2} = [S_2]/[S_1]^2$	statistical factor = 1/2
$K_{12,3} = [S_3]/[S_1][S_2]$	statistical factor = 2/2
$K_{13,4} = [S_4]/[S_1][S_3]$	statistical factor = 4/1

The component concentrations can be written as

$$[S_2] = K_{11,2}[S_1]^2 = 1/2K'_{11,2}[S_1]^2$$

$$[S_3] = K_{12,3}[S_1][S_2] = K_{11,2}K_{12,3}[S_1]^3 = (1/2)K'_{11,2}K'_{12,3}[S_1]^3$$

$$[S_4] = K_{13,4}[S_1][S_3] = K_{11,2}K_{12,3}K_{13,4}[S_1]^4 = 2K'_{11,2}K'_{12,3}K'_{13,4}[S_1]^4$$

In general, Y_Q is the ratio $4[S_4]/([S_1] + 2[S_2] + 3[S_3] + 4[S_4])$. By defining a numerator N and denominator D and letting $Y_Q = N/D$, one obtains

$$1 - Y_Q = (D - N)/D$$

$$Y_Q/(1 - Y_Q) = N/(D - N)$$

The ligand binding fraction in this case is

$$Y_Q/(1 - Y_Q) = 4[S_4]/([S_1] + 2[S_2] + 3[S_3])$$

$$= 8K'_{11,2}K'_{12,3}K'_{13,4}[S_1]^3/(1 + K'_{11,2}[S_1] + (3/2)K'_{11,2}K'_{12,3}[S_1]^2)$$

2. Duplex + Duplex Condensation in Terms of Quadruplex Formed with Simultaneous Triplex Formation. The subreactions are

$$(1)\ S_1 + S_1 \leftrightarrow S_2$$

$$(2)\ S_1 + S_2 \leftrightarrow S_3$$

$$(3)\ S_2 + S_2 \leftrightarrow S_4$$

The apparent equilibrium constants are

$K_{11,2} = [S_2]/[S_1]^2$	statistical factor = 1/2
$K_{12,3} = [S_3]/[S_1][S_2]$	statistical factor = 2/2
$K_{22,4} = [S_4]/[S_2]^2$	statistical factor = 2/1

The ligand binding fraction is

$$Y_Q/(1 - Y_Q) = 4[S_4]/([S_1] + 2[S_2] + 3[S_3])$$

$$= 16K'^{2}_{11,2}K'_{22,4}[S_1]^3/(1 + 4K'_{11,2}[S_1] + 6K'_{11,2}K'_{12,3}[S_1^2])$$

3. Stepwise Strand Addition and Duplex + Duplex Condensation in Terms of Quadruplex Formed. The subreactions are

$$(1)\ S_1 + S_1 \leftrightarrow S_2$$

$$(2)\ S_1 + S_2 \leftrightarrow S_3$$

$$(3a)\ S_1 + S_3 \leftrightarrow S_4$$

$$(3b)\ S_2 + S_2 \leftrightarrow S_4$$

The apparent equilibrium constants are

$K_{11,2} = [S_2]/[S_1]^2$	statistical factor = 1/2
$K_{12,3} = [S_3]/[S_1][S_2]$	statistical factor = 2/2
$K_{13,4} = [S_4]/[S_1][S_3]$	statistical factor = 4/1
$K_{22,4} = [S_2]/[S_1]^2$	statistical factor = 2/1

The the ligand binding fraction is

$$Y_Q/(1 - Y_Q) = 4[S_4]/([S_1] + 2[S_2] + 3[S_3])$$

$$= \{[4\gamma_4 K'_{11,2}K'_{12,3}K'_{13,4} + 16(\gamma - 1)K'^{2}_{11,2}K'^{2}_{22,4}][S_1]^3\}/(1 + 4K'_{11,2}[S_1] + 6K'_{11,2}K'_{12,3}[S_1]^2)$$

where γ is a "gating factor".

SUPPORTING INFORMATION AVAILABLE

^{1}H NMR spectrum of [d(TG_4)$_4$] in 100 mM Tris-HCl (pH 7), 100 mM KCl, and 0.1 mM EDTA at 23 °C (2 pages). Ordering information is given on any current masthead page.

REFERENCES

Bernardi, G. (1989) The isochore organization of the human genome. *Annu. Rev. Genetics 23*, 637−661.

Borman, S. (1994) Study Suggests Telomerase Inhibitors Could Be Effective Anticancer Drugs. *Chem. Eng. News*, April 25, pp 42−44.

Boynton, A. L., McKeehan, W. L., & Whitfield, J. F., Eds. (1982) *Ions, Cell Proliferation and Cancer*, Academic Press, New York.

Bustamante, J. O. (1993) Restricted ion flow in the nuclear envelope of cardiac myocytes. *Biophys. J. 64*, 1735−1749.

Cantor, C. R., & Schimmel, P. S. (1980) *Biophysical Chemistry*, Freeman, San Francisco.

Cantor, C. R., & Tinoco, I., Jr. (1965) Absorbance and optical rotary dispersion of seven trinucleoside diphosphates. *J. Mol. Biol. 13*, 65−77.

Cantor, C. R., Warshaw, M. M., & Shapiro, H. (1970) Oligonucleotide interactions. III. Circular dichroism studies of the conformation of deoxynucleotide. *Biopolymers 9*, 1059−1077.

Changeux, J.-P., & Rubin, M. M. (1968) Allosteric interactions in aspartate transcarbamylase. III. Interpretation of Experimental Data in Terms of the Model of Monod, Wyman, and Changeux. *Biochemistry 7*, 553−561.

Cheong, C., & Moore, P. B. (1992) Solution Structure of an Unusually Stable RNA Tetraplex Containing G- and U-Quartet Structures. *Biochemistry 31*, 8406−8414.

Cornish-Bowden, A., & Koshland, D. E., Jr. (1970) The influence of binding domains on the nature of subunit interactions in oligomeric proteins. *J. Biol. Chem. 245*, 6241−6250.

Cornish-Bowden, A., & Koshland, D. E., Jr. (1975) Diagnostic uses of the Hill (Logit and Nernst) plots. *J. Mol. Biol. 95*, 201−212.

Coviello, G. M., Wright, W. E., Weinreich, S. L., & Shay, J. W. (1994) Specific association of human telomerase activity with immortal cells and cancer. *Science 266*, 2011−2015.

Davis, C. R., & Tinoco, I., Jr. (1968) Temperature-dependent properties of dinucleoside phosphates. *Biopolymers 6*, 223−242.

Deng, H., & Braunlin, W. H. (1995) Duplex to quadruplex equilibrium of the self-complementary oligonucleotide d(GGGGCCCC). *Biopolymers 35*, 677−681.

Dill, K. A. (1990) Dominant Forces in Protein Folding. *Biochemistry 29*, 7133−7155.

Fang, G., & Cech, T. R. (1993a) The β subunit of Oxytricha telomere-binding protein promotes G-quartet formation by telomeric DNA. *Cell 74*, 875−885.

Fang, G., & Cech, T. R. (1993b) Characterization of a G-Quartet Formation Reaction Promoted by the β Subunit of the Oxytricha Telomere-Binding Protein. *Biochemistry 32*, 11646−11657.

Fearon, E. R., & Vogelstein, B. (1990) A genetic model for colorectal tumorigenesis. *Cell 61*, 759−767.

Fromm, H. J. (1975) *Initial Rate Enzyme Kinetics*, Springer-Verlag, New York.

Giraldo, R., & Rhodes, D. (1994) The yeast telomere-binding protein RAP1 binds to and promotes the formation of DNA quadruplexes in telomeric DNA. *EMBO J. 13*, 2411−2420.

Glaser, R., & Gabbay, E. J. (1964) Topography of nucleic acid helices in solutions. II Interactions of spermine and spermidine derivatives with polyadenylic-polyuridylic and polyinosinic-polycytidylic acid helices. *Biopolymers 6*, 243−254.

Gomez, J., & Friere E. (1995) Thermodynamic mapping of the inhibitor site of the aspartic protease endothiapepsin. *J. Mol. Biol. 252*, 337−350.

Guo, Q., Lu, M., & Kallenbach, N. R. (1993) Effect of Thymine Tract Length on the Structure and Stability of Model Telomere Sequences. *Biochemistry 32*, 3596−3603.

Hardin, C. C., Henderson, E., Watson, T., & Prosser, J. (1991) Monovalent Cation-Induced Structural Transitions in Telomeric DNAs: G-DNA Folding Intermediates. *Biochemistry 30*, 4460−4472.

Hardin, C. C., Watson, T. Corregan, M., & Bailey, C. (1992) Cation-Dependent Transition between the Quadruplex and Watson−Crick Hairpin Forms of d(CGC G_3 GCG). *Biochemistry 31*, 833−841.

Hardin, C. C., Corregan, M., Brown, B. A., II, & Frederick, L. (1993) Cytosine·Cytosine Base-Pairing Stabilizes DNA Quadruplexes and Cytosine Methylation Greatly Enhances the Effect. *Biochemistry 32*, 5870−5880.

Hastie, N. D., Demster, M., Dunlop, M. G., Thompson, A. M., Green, D. K., & Allshire, R. C. (1990) Telomere reduction in human colorectal carcimona and with ageing. *Nature 346*, 866−868.

Henderson, E. R., & Blackburn, E. H. (1989) An overhanging 3′ terminus is a conserved feature of telomeres. *Mol. Cell. Biol. 9*, 345−348.

Hill, T. L. (1986) A theoretical study of cooperative dual linear aggregation and the vernier effect. *Biophys. Chem. 25*, 1−15.

Howard, F. B. & Miles, H. T. (1982) A stereospecific complex of poly (I) with ammonium ion. *Biopolymers 21*, 147−157.

Hud, N. V., Smith, F. W., Anet, F. A. L., & Feigon, J. (1996) The selectivity for K^+ versus Na^+ in DNA Quadruplexes Is Dominated by Relative Free Energies of Hydration: A Thermodynamic Analysis by ^{1}H NMR. *Biochemistry 35*, 15383−15390.

Jin, R., Breslauer, K. J., Jones, R. A., & Gaffney, B. L. (1990) Tetraplex formation of a guanine-containing nonameric DNA fragment. *Science 250*, 543−546.

Kandimalla, E. R., & Agrawal, S. (1995) Single strand targeted triplex-formation. Destabilization of guanine quadruplex structures by foldback triplex-forming oligonucleotides. *Nucleic Acids Res. 23*, 1068−1074.

Kauffman, S. A. (1993) *The Origins of Order*, Oxford Press, 709 pp.

Kim, N. W., Piatyszek, M. A., Prowse, K. R., Harley, C. B., West, M. D., Ho, P. L. C., Koshland, D. E., Jr., Nemethy, G., & Filmer, G. (1966) Comparison of Experimental Binding Data and Theoretical Models in Proteins Containing Subunits. *Biochemistry 5*, 365−385.

Ling, G. N. (1984) *In Search of the Physical Basis of Life*, Plenum Press, New York.

Marky, L. A., & Breslauer, K. J. (1987) Calculating Thermodynamic Data for Transitions of Any Molecularity from Equilibrium Melting Curves. *Biopolymers 26*, 1601−1620.

Mazzanti, M., DeFelice, L. J., & Smith, E. F. (1991) Ion channels in murine nuclei during early development and in fully differentiated adult. *Membr. Biol. 121*, 189−198.

Miura, T., Benevides, J. M., & Thomas, G. J., Jr. (1995) A phase diagram for sodium and potassium ion control of polymorphism in telomeric DNA. *J. Mol. Biol. 248*, 233−238.

Olivas, W. M., & Maher, L. J., III (1995) Competitive Triplex/Quadruplex Equilibria Involving Guanine-Rich Oligonucleotides. *Biochemistry 34*, 278−284.

Record, M. T., Jr., Lohman, T. M., & de Haseth, P. (1976) Ion effects on ligand nucleic acid interactions. *J. Mol. Biol. 107*, 145−158.

Ross, W. S., & Hardin, C. C. (1994) Ion-Induced Stabilization of the G-DNA Quadruplex: Free Energy Perturbation Studies. *J. Am. Chem. Soc. 116*, 6070−6080.

Sarma, M. H., Luo, J., Umemoto, K., Yuan, R., & Sarma, R. H. (1992) Tetraplex formation of d(GGGGGTTTTT): ^{1}H NMR study in solution. *J. Biomol. Struct. Dynam. 9*, 1131−1153.

Schultz, S. *et al.* (1997) Described in seminar by Prof. T. R. Cech, Duke University, Nov. 7, 1995; see http://www.Colorado.EDU/Chemistry/grad/faculty/Schultz/Schultz.html.

Sen, D., & Gilbert, W. (1990) A potassium switch in the formation of four-stranded G4-DNA. *Nature 344*, 410−414.

Singleton, S. F., & Dervan, P. B. (1993) Equilibrium Association Constants for Oligonucleotide-Directed Triple Helix Formation at Single DNA Sites: Linkage to Cation Valence and Concentration. *Biochemistry 32*, 13171−13179.

Venczel, E. A., & Sen, S. (1996) Synapsable DNA. *J. Mol. Biol. 257*, 219−224.

Vesnaver, G., & Breslauer, K. J. (1991) The contribution of DNA single-stranded order to the thermodynamics of duplex formation. *Proc. Natl Acad. Sci. U.S.A. 88*, 3569−3573.

Wang, Y., & Patel, D. J. (1992) Guanine Residues in d(T_2AG_3) and d(T_2G_4) Form Parallel-Stranded Potassium Cation Stabilized G-Quadruplexes with Anti Glycosidic Torsion Angles in Solution. *Biochemistry 31*, 8112−8119.

Williams, A. P., Longfellow, C. E., Freier, S. P., Kierzek, R., & Turner, D. H. (1989) Laser Temperature-Jump, Spectroscopic, and Thermodynamic Study of Salt Effects on Duplex Formation by dGCATGC. *Biochemistry 28*, 4283−4291.

Williamson, J. R. (1994) G-quaret structures on telomeric DNA. *Annu. Rev. Biophys. Biomol. Struct. 23*, 703−730.

Wyatt, J. R., Davis, P. W., & Freier, S. M. (1996) Kinetics of G-Quartet-Mediated Tetramer Formation. *Biochemistry 35*, 8002−8008.

Wyman, J., & Gill, S. J. (1990) *Binding and Linkage*, University Science Books, Mill Valley, CA.

Xu, Q., Deng, H., & Braunlin, W. H. (1993) Selective Localization and Rotational Immobilization of Univalent Cations on Quadruplex DNA. *Biochemistry 32*, 13130−13137.

BI970488P